FISEVIER

Contents lists available at ScienceDirect

Materials Today Communications

journal homepage: www.elsevier.com/locate/mtcomm



Effect of particle size distribution on the packing of powder beds: A critical discussion relevant to additive manufacturing



Alessandro Averardi, Corrado Cola, Steven Eric Zeltmann, Nikhil Gupta*

Composite Materials and Mechanics Laboratory, Mechanical and Aerospace Engineering Department, Tandon School of Engineering, New York University, Brooklyn, NY, 11201, USA

ARTICLE INFO

Keywords: Additive manufacturing 3D printing Selective laser sintering Selective laser melting Electron beam additive manufacturing Particle packing

ABSTRACT

Several additive manufacturing (AM) methods use powder feed materials. Selective laser sintering is an example of a versatile AM method, using feed material in powder form, capable of producing polymer and metallic parts. In the variations of this technique, a laser spot or an electron beam is used to locally sinter or melt a packed powder bed. After the completion of sintering on each layer, further powder is added on top of the existing bed so that the next layer may be joined. A major challenge in this method is controlling the porosity of the powder bed so that the final part has uniform and maximum density. Uniformity in the packing of bed from one layer to the other is important for optimizing the processing parameters. This review is focused on considering the packing characteristics of polydisperse hard particle beds and the determination of the expected density achievable for a given particle size and shape distribution. Models are presented for discrete mixtures as well as continuous distributions. The effect of the initial configuration of a particle bed on its ability to form a highly dense packing is also discussed. Blending of different particle sizes and shapes can be used to substantially increase the packing density, but can also lead to separation or segregation of the bed. Through appropriate control of the particle shape and use of wide distributions, packing densities close to 100 % can theoretically be achieved, but practicality and various effects that appear at small size scales prevent from achieving such high packing densities. Recent advancements have reduced the dependence of AM part quality on the density of the packed particle bed but the packing is still important for considerations such as thermal conductivity of the bed and absorption of laser power in the bed. Improved knowledge of packed bed characteristics can be helpful in developing AM methods for novel material systems.

1. Introduction

Additive manufacturing (AM) is one of the fastest growing industrial fields in the current times. Initially used for prototyping, AM methods are now mainstream production methods for many aircraft components [1,2], spacecraft components [3,4], medical devices [5,6], and consumer products [7]. Technically, any technique that manufactures a part layer by layer can be classified under the umbrella of AM. ISO/ASTM 52,900 is widely used to define seven categories of AM methods [8], which include binder jetting, direct energy deposition, material extrusion, material jetting, powder bed fusion, sheet lamination and vat polymerization. Further variation in these processes have now resulted in a suite of over 50 different possible AM technologies. Each of these categories has some techniques that have become commercially viable while some other techniques are in the nascent stage of development for the next generation manufacturing method. Fused filament fabrication

methods have gained wide commercial success due to low cost printers and ease of printing parts. However, these methods are mostly used for prototyping and by hobbyists. Powder based methods have emerged to manufacture industrial grade components that can be deployed in real application. Therefore, a significant effort is ongoing to understand the effect of various processing parameters on the quality of the printed part in these methods.

Since powder bed methods are based on creating a layer of powder on the build plate and then sintering that powder to make the shape by repeating the process in successive layers hundreds or even thousands times, the characteristics of the powder bed are very important for many reasons. Spherical powders are used as the feed materials, where the particles can be of the same size or have a size distribution. The packing of spherical particles always has some porosity present in the interparticle spaces. In addition to density [9], the packing characteristics of powder in the bed also determine the heat transfer

^{*} Corresponding author.

E-mail address: ngupta@nyu.edu (N. Gupta).

characteristics of the bed and flow of molten material due to heating [10]. Minimization of porosity can be beneficial in obtaining a stable bed and stable melt pool during printing process. In addition, effective thermal conductivity of highly packed beds is higher than that of the lower packing arrangements. However, porosity allows gases to escape from the bed, which is useful in minimization of porosity in the printed part due to entrapped gases [11,12] and the convective and radiative heat transfer can be increased by having greater porosity in the bed of particles of insulating nature or reflective surface [13]. It is apparent that some of the requirements for the packed beds are conflicting and the development of processing parameters requires understanding the parameters that affect packing of particles of different types.

Rapidly increasing applications of AM methods in manufacturing deployment quality parts in aerospace, medical and automotive sectors have inspired studies to analyze the effects of processing parameters on the quality of additive manufactured parts [14-16]. The effect of laser power, scanning speed, and powder bed layer thickness have been studied on parameters such as porosity in the printed part, surface roughness, and microstructure [11,17]. Density of the packed bed is another parameter of critical importance as outlined by many studies [18,19] but is among the least understood parameter in this field. It is well known that the particles of the same size can provide close-packed arrangement providing 74 % packing by volume. However, in large beds, the arrangement is not close-packed and all particles are not of same size. Understanding the effect of parameters such as particle size distribution and shape can help in developing beds that can provide high quality additive manufactured parts. Thermal characteristics are also shown to be strongly dependent on the particle packing in the bed. For example, it is shown for AlSi10Mg processed by laser melting process that the peak temperature of the melt pool decreased from about 2500 K to about 2,300 K as the porosity of the powder bed decreased from 0.45 to 0.3 due to decrease in the effective thermal conductivity of the bed [20]. In the bed of highly reflective AlSi10Mg alloy particles, convection plays an important role and decrease in conductivity reduces the effective heat transfer, resulting in a shallower melt pool and poor bonding between scan track and the substrate. The characteristics of steel particle beds may be different because of highly absorbing nature of the steel particles. An improved understanding of particle packing can help in resolving such issues.

The present review focuses on the powder bed technologies, which currently form the most important class of AM methods because of their industrial scale production capabilities. Powder bed AM methods rely on creating a thin bed of powder on which a laser or electron beam is used to sinter or melt the powder in a specific shape. The next powder layer is deposited on top of the previous one and the process continues until the entire part is built. This process can be used with any material that can be melted and resolidified and examples can be found in polymers, metals, and ceramics for use with these methods. Many of the current commercially successful parts manufactured by AM have used powder bed fusion technologies. For example, the GE LEAP fuel nozzle is made by this kind of processing method. Deep interest in the development of these methods for obtaining parts that are as good as those manufactured by traditional methods such as casting has resulted in studies related to all aspects of the processing, including developing tailored raw materials, processing conditions, and post-manufacturing evaluation to feed the information back into the manufacturing method for continuous improvement.

The major challenge in powder bed technologies is to eliminate porosity in the printed part by means of powder design and processing parameter optimization [21]. Many printed parts are subjected to hot isostatic pressing (HIP) after printing to completely eliminate the porosity [22–24]. However, additional steps cost time and money and are undesired. In addition, dimensions of the printed parts change during porosity compaction during HIP, compromising dimensional tolerances. Therefore, the importance of raw material design and understanding the characteristics of packed beds is paramount in this field. Imaging

methods are being use to understand the packing of particles in beds to find defects in packing and correlate them to the printed part quality [25]. Improving the packing of particle beds can significantly reduce the defects such as gas pores and improve the heat transfer characteristics of the bed to obtain a more uniform heat distribution. Studies are also available to estimate the thermal conductivity of packed particle beds to understand the heat distribution characteristics [26–29]. Hence, understanding the packing of particles of different size distributions is of extreme importance in this field, which is the focus of this review. This review does not cover the details of various AM methods and particle production methods [30,31], on which ample recent literature is available in the form of review articles and books [32–36]. However, fundamental understanding of particle packing in beds is still scattered across numerous fields and needs consolidation.

The science of powder packing is not new. Problems of powder packing have been studied in a number of fields for decades. For example, sand casting [37], phase separation of fluids [38], filtration [39], porous media for heat exchange [40], pharmaceutical tablet manufacturing [41,42], sound absorption [43], particulate composites [44,45] and packaging material development are a few examples among numerous fields where information on particle packing has been studied [46,47]. The existing knowledge from these fields can provide an informed basis for developing packed beds for AM. The starting point for most of this information is relatively simple: that the same size spheres at closed-packing arrangement provide 74 % packing, whereas the same set of spheres at random closed-packing provides about 63 % space filling [48]. It is desirable to have beds as close-packed as possible and meet or exceed at least the random close-packing efficiency. With 74 % being the upper limit for any set of same size spherical particles, methods are required to increase the initial packing efficiency to have beds with lower starting porosity. Creating a size distribution of spherical particles and changing the shape are among the possibilities that have been extensively studied in various fields, which is the focus of the present review. The study of the particle size and shape effects is also relevant to fabricating parts of composite materials using AM.

Composite materials are an important class of materials for industrial applications. Metal matrix composites with ceramic reinforcements are widely used and components made of composites are now being developed using AM methods [49–53]. Matching of shape and size of particles of matrix and reinforcement is a great challenge because of their different material properties and atomic bonding. Spherical metal powders can be produced but ceramics powders may vary in their particle morphology. In such cases, development of a scheme that can predict the packing efficiency of mixed powder is a challenging problem because of difficulty in predicting the packing of non-spherical particles.

The remainder of this review is structured as follows: Section 2 discusses the classical results on the random packing of particle beds, including their formation and stability. Section 3 discusses the mathematical treatment of discrete particle distributions, that is, packings of systems where particles fall into a finite number of discrete size classes. These packings can be studied in-depth by analytical methods, and the available experiments match closely with the empirical treatment. Section 4 considers the more complicated case where the particle system is characterized by a continuous distribution of sizes; this type of system cannot be analyzed using the analytical geometry and linear systems theory used in the discrete case, and so can only be treated approximately. However, such treatment is highly important in practical cases due to the relative ease of measuring particle size distributions. Modern equipment can measure the size and shape of millions of particles per second to provide highly accurate characterization of size distributions. Convenient means of estimating the packing properties of such measured distributions are discussed. In Section 5, the small scale physical effects that disrupt ideal packing, such as Van der Waals and electrostatic forces, are discussed and computer simulations on their impact on packing are discussed. Section 6 discusses the effects related

to small particles, especially that the interparticle bonding becomes important when the particles are below a critical size, leading to lower packing efficiency than anticipated. Implications of particle bed packing efficiency on the selective laser sintering (SLS) are discussed in Section 7. Finally, summary of the findings of this critical review is presented in Section 8, along with future outlook.

2. Random monodisperse packings

If spheres of uniform size, i.e. monodisperse spheres, are poured into a container and tapped or vibrated to cause them to settle, they are observed experimentally to achieve packing densities of between 0.60 and 0.64¹. In a classic paper on packing of uniform spheres, McGeary tested the packing of lead, sulfur, and steel shot, steel ball bearings, glass beads, rounded sand, round California beans, and poppy seeds and found that they all produced packing densities in this range and that for each material the packing density was repeatable to less than 1 % between experiments [54]. In the monodisperse case, it is possible to identify a number of simple regular packing patterns. From solid geometry, there are four possible packings: simple cubic, orthorhombic, double-nested, and close-packed. These structures yield packing fractions of $\varphi = 60.46$ %, 69.81 %, and 74.05 %, with double-nested and close-packed having the same packing fraction. Simple cubic packing is not stable under agitation — if the layers are allowed to move against one another they will settle into the orthorhombic arrangement. The three stable arrangements are shown in Fig. 1.

In McGeary's experiments, the particle beds were observed to be composed mostly of the orthorhombic arrangement. However, some regions of the denser arrangements were present, allowing the packing fraction to exceed the $\approx\!60$ % packing density for orthorhombic. While the "single-nested" orthorhombic arrangement can be produced by vertical settling (such as caused by horizontal shearing forces) of the particle bed, the "double-nested" arrangement arises when this is coupled with shearing in an orthogonal plane to produce further nesting of layers. Since this arrangement packs at $\approx\!70$ %, it is estimated that about 20 % of the particles in these experiments were in the double-nested arrangement. Close-packed structures, or "triple-nested," were not observed in the experiments and it was hypothesized that their formation would involve displacements to nearby layers that would propagate and reinforce the double-nesting.

Obtaining perfectly regular packings of any structure is essentially impossible experimentally for large numbers of particles which are filled randomly in the container. Because of the difficulty in assessing any particular structure, most literature instead refers to "random close packing," or the maximally dense packing obtainable by tapping or vibrating a randomly filled bed [48,55,56]. This "structure" is abbreviated as rcp, and the density is represented as φ_{rcp} . Conversely, the initial state before any tapping, which is stable but has minimal density, is referred to as loose packing. There are numerous standards which assign labels such as "loose," "medium," or "dense" packing depending on the density or on the specific procedure which was used to tap or shake the bed [57], and based on the particle size distributions measured through sieving [58]. These definitions are mainly of interest in civil engineering, as the response of soils varies considerably with density, and reproducible methods are needed to produce uniform samples for testing. Random close pack densities were experimentally measured in [59] for steel balls in air, steel balls in paraffin oil, polished Plexiglas balls in air and nylon balls with a ground surface. These results are shown in Table 1. Neither the Plexiglas nor the nylon balls were as uniform or as spherical as the steel balls. The effects of surface roughness and lubrication on the attainable density is dependent on

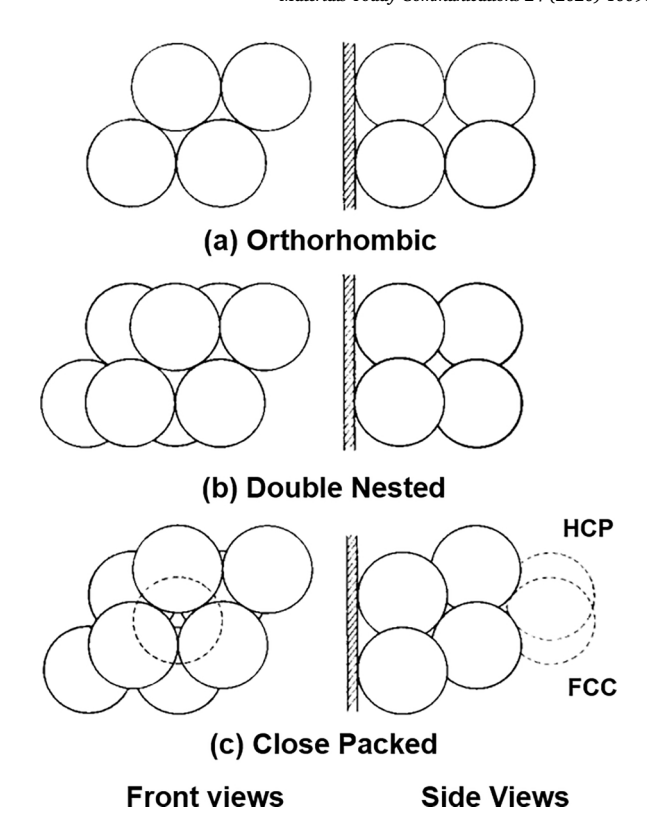


Fig. 1. Regular arrangements of monodisperse spheres: (a) orthorhombic, (b) double nested and (c) close packed. Reused with permission from [54].

Table 1
Random close packed densities measured by [59].

Particle material	Loose	Close packed	
Steel balls	0.608	0.638	
Steel (in oil)	0.611	0.636	
Plexiglass (polished)	0.605	0.630	
Nylon (ground)	0.575	0.629	

inter-particle interactions that may impede the nesting of layers.

These measurements have been repeated by many authors and generally have shown repeatability for each material of better than 1 % [55,60]. If the hypothesized sources of error, which prevent reaching the ideal rcp structure, are accounted for the results of different materials converge. Thus, the accepted density for the density of the random-close packing of spheres is $\varphi_{rcp} = 0.6366 \pm 0.0005$. Shape and size of the container also influence packing density. For practical purposes, maximum packing density can be obtained if the container diameter is at least an order of magnitude larger than the sphere diameter [54,61,62]. For a cylindrical container, layers of spheres consisting in concentric circles arranged in almost completely rhombic pattern were observed. Containers with a square cross-section caused a predominately square pattern in the surface spheres viewed through the transparent container wall, although numerous colonies of rhombic pattern and random arrangement were observable. The important fact is that approximately the same packing density has been attained for all these packings and its value agreed very closely with other experimental results. The suggested explanation for this circumstance is that the three-dimensional packing arrangement was really the same and mainly orthorhombic.

3. Linear models of polydisperse packings

In the case of polydisperse packings, solid geometry approaches are

 $^{^1}$ The packing density ϕ is defined as the solid volume of the spheres (or any objects inside the packing) divided by the total volume they occupy. Note that many older studies report the porosity, which is equal to $1-\phi$.

generally intractable except for the simplest cases. Instead, the linear model theory of particle packing is applied, which can be adapted to any arbitrary discrete distributions of particles. This model considers a system composted of n equal density, spherical particles having diameter d_i and solid volume S_i . The specific volume of each particle V_i is the ratio of the apparent volume occupied to its solid volume, and is equal to the reciprocal packing fraction of that particle, φ_i^{-1} . The fractional solid volume X_i of each particle is its solid volume divided by the total solid volume of all particles,

$$X_i = \frac{S_i}{\sum_{i=1}^n S_i} \tag{1}$$

and so satisfies the constraints

$$\sum_{i=1}^{n} X_i = 1 \cap X_i \ge 0 \ \forall_i = 1,, n$$
 (2)

The apparent total volume of the packing V^T is a function of V_i , S_i , and d_i , which can be written according to Euler's theorem as

$$V^{T} = f(V_{i}, S_{i}, d_{i}) = \sum_{i=1}^{n} S_{i} \left(\frac{\partial V^{T}}{\partial S_{i}} \right)_{V, d, S_{j}} = \sum_{i=1}^{n} S_{i} V'_{i}$$
(3)

where V_i is defined as the partial specific volume of particle i. This can be interpreted as the change in total volume of the packing when the particle i is added to an already large volume packing. The specific volume of the packing is then

$$V = \frac{V^T}{\sum_{i=1}^n S_i} = \sum_{i=1}^n X_i V_i$$
 (4)

What is missing from this simple statement of the model is the form of $f(V_i,\underline{Si},d_i)$, which contains the information on the interactions between particles. These interactions must also be a function of the entire packing, rather than simply a function of the individual components only. Delving into the various realizations of this function is beyond the scope of this review, so only the results of this model will be considered here. In the following subsections, various "special" discrete distributions which have interesting and practically useful properties are discussed.

3.1. Maximally dense discrete mixtures

Graton and Fraser studied the packing structure of binary mixtures [63], and identified two different regimes of packing behavior based on the size ratio between the two components. These results are shown in Fig. 2 [64], and it is clear that there is a change in the packing mechanism across a critical size ratio. The size ratio ρ at which the transition happens was found to be $\approx\!1.35^3$ and was termed the "ratio of replacement." For size ratios smaller than this value, the total volume is mostly insensitive to the relative fraction of each component since the smaller particles can effectively "replace" the larger ones in the packing. At greater size ratios, the smaller particles can fit in the (distorted) interstitial positions of the larger particle packing structure, leading to higher packing density (lower specific volume) and a strong sensitivity of the packing density to the relative fraction of each component.

If the size ratio is increased further to \approx 6.5, the gaps between the large particles become large enough that the smaller particles can fill the spaces without substantially distorting the larger particle packing structure. This size ratio is called the "ratio of entrance" [54], above which packing occurs due to the "filling mechanism." This is due to the

ability of the smaller size particles to fill the interstitial sites of the larger particle packing without disrupting it. Below this size ratio, the "occupation mechanism" dominates, and mutual interaction between the components creates a less ordered and less dense packing.

Simulation studies have shown the possibility of creating jammed sphere packings with a wide variation in density of the packed beds. Local order affects the density of the large scale packed beds and packing densities could obtained as low as 0.52 and as high as the fcc packing density of 0.74 [65]. In further work, the Lubachevsky-Stillinger (L-S) model was modified to introduce the effect of particle size polydispersivity [66]. In this case, a random particle dispersion was allowed to grow at the rate proportional to the initial particle radius until a jammed packed state was obtained. It was observed that the polydisperse systems tend to remain amorphous over a broader range of packing fractions. The modified L-S algorithm predicted packing density of binary systems to be similar to the results obtained from Monte Carlo simulations at small volume ratios (ratio of large particle to small particle volumes). For large volume ratios, the predictions of modified L-S algorithm was similar to the experimental observations [66]. The prediction of viscosity of systems filled with monodispersed and bimodal distribution of particles has been used to estimate the packing fraction of the particles [67]. The maximally random jammed (MRJ) packing fraction for the monodisperse particle is found to be 0.634 but this parameter for bimodal systems depends on the sphere diameter ratio and the fraction of small particles in total solids [68]. In silica filled mixtures used for ceramic stereolithography, using bimodal distribution displays most significant decrease of suspension viscosity than suspension made of the same size particles [69].

The filling mechanism of packing presents an opportunity to design optimally dense multi-component packings. This is achieved by adding successive particle sizes to the distribution, each having a size ratio equal to the ratio of entrance. Thus, each successive component will fill the interstitial sites in the next largest distribution. Each successive component will add to the total volume of particles without disrupting the packing of the larger particles and thus without increasing the total volume of the packing. If *m* different particle sizes are used, each differing by the ratio of entrance, it follows that the total packing density of the bed will be [70]

$$\phi_{max} = \phi_1 + (1 - \phi_1)\phi_2 + \dots + (1 - \phi_1)(1 - \phi_2)\dots(1 - \phi_{m-1})\phi_m$$
 (5)

Since all of the factors are less than unity and decay rapidly, each successive particle size added to the distribution will have diminishing contribution to the maximum packing fraction. The required relative fraction of each component of this mixture can be determined by dividing Eq. 6 by φ_{max}

$$1 = \frac{\phi_1}{\phi_{max}} + \frac{(1 - \phi_1)\phi_2}{\phi_{max}} + \dots + \frac{(1 - \phi_1)(1 - \phi_2)\dots(1 - \phi_{m-1})\phi_m}{\phi_{max}}$$

$$= X_1^* + X_2^* + \dots + X_m^*$$
(6)

Only knowledge of the individual initial packing densities is required to calculate the composition of maximum density. If it is assumed that $\varphi_1=0.63$, such that each component attains the random close packed density, then an upper limit for the maximum packing density of the mixture [71,72], as well as its composition, is predicted using Eqs. 5 and 6, as shown in Table 2.

It is interesting to note that, according to McGeary [54], the maximum packing fraction could be obtained by only one experimental technique. The coarse component by itself was vibrated until it attained a minimum volume. Vibration was stopped, and the fine component was poured into the container and vibration continued until a minimum volume was again attained. Lower final packing density resulted when the components were blended, poured into the container, and vibrated. In fact, there was gross segregation after attempted blending.

² The requirement of equal density is purely a practical one, to prevent separation due to buoyancy effects in experimental packing.

 $^{^3}$ In this review, the size ratio ρ will consistently be defined as large/small, since it is more physically intuitive.

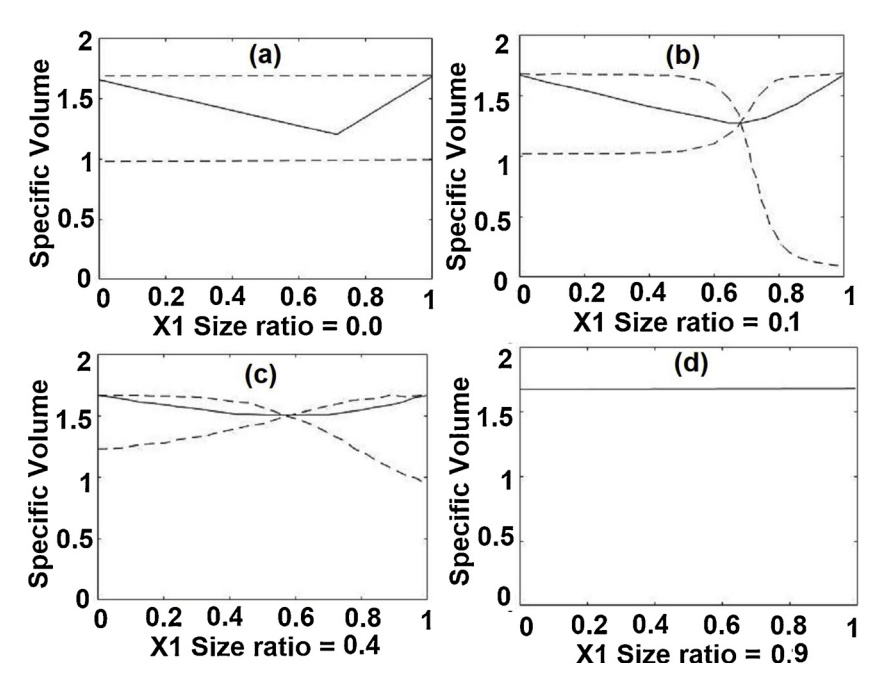


Fig. 2. Specific volume of binary mixtures (continuous line) and partial specific volume of components (dashed lines) versus component size ratio plotted for X1 size ratio of (a) 0.0, (b) 0.1, (c) 0.4 and (d) 0.9. Note that the size ratio on the plot axes is defined as small/large, or ρ^{-1} using the definition in this work [63]. Figure is reused with permission [63]. The figure is reused with permission from [64].

Table 2Component fractions for a maximally dense bed, with each differing in size by the ratio of entrance [70].

Number of components	φ_{max}	<i>X</i> ₁ *	<i>X</i> ₂ *	X ₃ *	X ₄ *	<i>X</i> ₅ *
1	0.63	1.0				
2	0.86	0.73	0.27			
3	0.95	0.67	0.25	0.09		
4	0.98	0.64	0.24	0.09	0.04	
5	0.99	0.64	0.23	0.08	0.03	0.01

3.2. Arbitrary binary mixtures

In the previous section, estimations of the packing of the bed were only possible under the assumption that each size of particle effectively saw an unconstrained environment to fill. This is because of the difficulties associated with expressing the function that defines the packing. In this section, an empirical model is described which yields good predictions for binary mixtures, with no restriction on the size ratio. Westman introduced this relationship between the specific volume and the fractional solid volumes X_1 and $X_2 = 1 - X_1$, which is based on a conic equation [72,73]:

$$\left(\frac{V - V_1 X_1}{V_2}\right)^2 + 2G\left(\frac{V - V_1 X_1}{V_2}\right) \left(\frac{V - X_1 - V_2 X_2}{V_1 - 1}\right) + \left(\frac{V - X_1 - V_2 X_2}{V_1 - 1}\right)^2
= 1$$
(7)

where *G* is an empirically determined coefficient. Fig. 3 shows the porosity of binary mixtures computed using Eq. 7, along with experimental results [64]. The maximum packing density predicted is $\varphi = 0.76$ for $\rho \to \infty$, which is the same result as that obtained in §3.1 and occurs at the same relative volume fractions.

In empirical studies, it is also found that the maximum packing density is also a function of the initial configuration of the particles, which can be quantified by the initial porosity ε_0 . The maximum contraction of the packing upon tapping or shaking $\Delta\varepsilon$ is a function of the size ratio and the initial porosity. In the case where $\rho \to \infty$, the maximum contraction is [74]

$$\Delta \varepsilon_o = \varepsilon^o (1 - \varepsilon^o) \tag{7}$$

A quadratic regression proposed by [71] and later modified by Ridgway and Tarbuck [75,76] is expressed as

$$\frac{\Delta \varepsilon_{max}(r)}{\Delta \varepsilon_o} = \begin{cases} 1 - 2.35r + 1.35r^2 r \le 0.741\\ 0 r > 0.741 \end{cases} \tag{8}$$

where $r = \rho^{-1}$, and is plotted against experimental results in Fig. 4 [74]. The minimum specific volume, or maximum packing density, is then

$$V_{min} = \frac{1}{1 - \varepsilon_{min}} = \frac{1}{1 - (\varepsilon^{o} - \Delta \varepsilon_{max})}$$
(9)

3.3. Polydisperse discrete distributions

Modeling of discrete polydisperse distributions with more than two components can be accomplished through an extension of the binary theories discussed above. Considering a system made of two components of different size *before mixing*, the specific volume of that system is

$$V = X_1 V_1 + X_2 V_2 \tag{10}$$

If the two components are then mixed, the specific volume of the system changes, which can be represented as

$$V = X_1 V_1 + X_2 V_2 + C_{12} X_1 X_2 (11)$$

 C_{12} is a coefficient that represents the joint action that results from mixing the two components. By manipulating Eq. 7 and joining with Eq. 11, C_{12} can be found as a function of ρ and $X_1 - X_2$. A plot of C_{12} for different size ratios as a function of $X_1 - X_2$ is shown in Fig. 5, and the relationship is approximately linear [64]. Therefore, the coefficient can be estimated using a linear equation

$$C_{12} = \beta_{12} + \gamma_{12}(X_1 - X_2) \tag{12}$$

Inserting this in Eq. 11 yields

$$V = X_1 V_1 + X_2 V_2 + \beta_{12} X_1 X_2 + \gamma_{12} (X_1 - X_2) X_1 X_2$$
(13)

The term $\beta_{12}X_1X_2 + \gamma_{12}(X_1 - X_2)X_1X_2$ is called the "synergism" of the mixture, and coefficients β_{12} and γ_{12} are found to be independent of initial specific volume and size ratio. A general formula to compute the specific volume of polydisperse mixtures was proposed by Scheffè et al. [77] considering n components

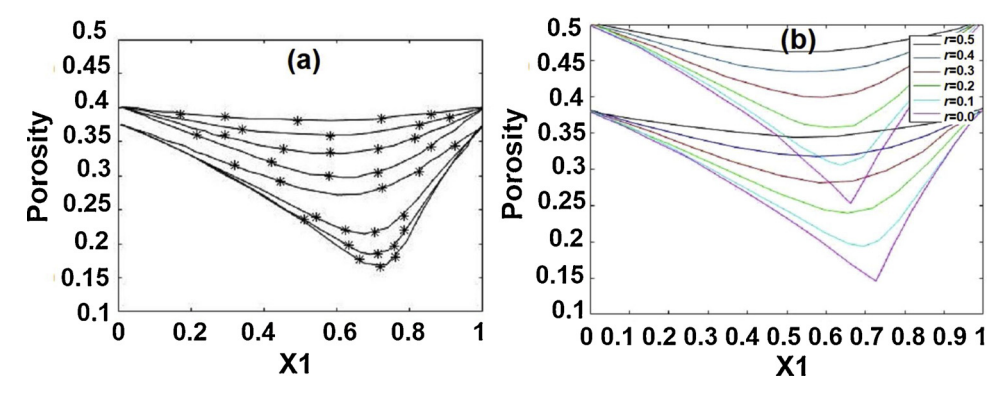


Fig. 3. Porosity $(1-\Phi)$ of binary mixtures as a function of X_1 , by (a) experiment and (b) Eq. 7. The numbers marked on the lines in (b) denote ρ^{-1} . The figure is reused with permission from [64].

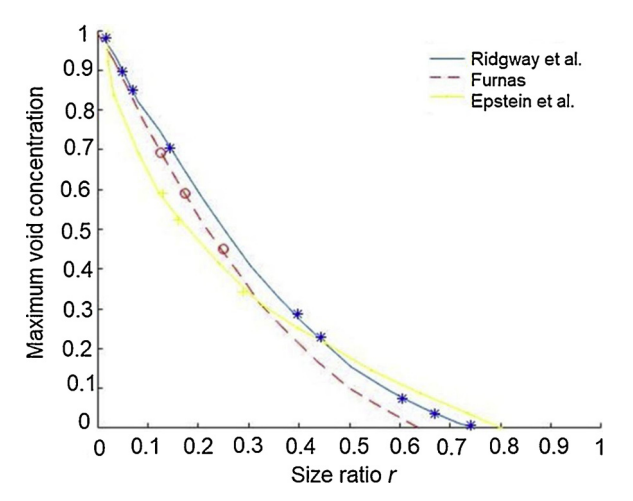


Fig. 4. Maximum void contraction versus (inverse) size-ratio. The figure is reused with permission from [74].

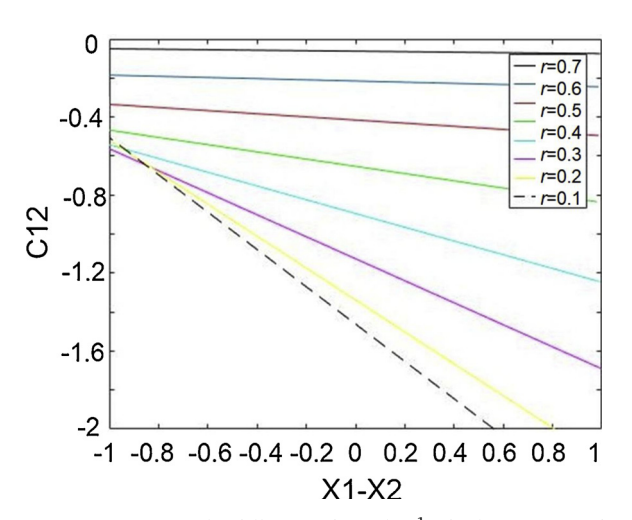


Fig. 5. C_{12} versus $X_1 - X_2$ for different values of ρ^{-1} . The figure is reused with permission from [64].

$$V = \beta_0 + \sum_{i=1}^n \beta_i X_i + \sum_{1 \le i_1 \le i_2 \le n} \beta_{i_1 i_2} X_{i_1} X_{i_2}$$

$$+ \dots + \sum_{1 \le i_1 \le i_2 \le \dots \le i_k \le n} \beta_{i_1, i_2, \dots, i_k} (X_{i_1}, X_{i_2}, \dots, X_{i_k})$$

$$(14)$$

To make this approach more tractable, it is generally assumed that there are no joint actions among any three or more components [64], so that the equation becomes

$$V = \sum_{i}^{n} \beta_{i} X_{i} + \sum_{1 \le i \le j}^{n} \beta_{ij} X_{i} X_{j} + \sum_{1 \le i \le j}^{n} \gamma_{ij} X_{i} X_{j} (X_{i} - X_{j})$$
(15)

Comparing to Eq. 13, it is found that $\beta_i=V_i$, and the values of β_{ij} and γ_{ii} are found by minimization of the function

$$\sum \left[\beta_{ij} + \gamma_{ij} (X_i - X_j) - \frac{V_{ij} - V_i X_i - V_j X_j}{X_i X_j} \right]^2$$
(16)

Using Eq. 16 it is possible to compute the specific volume of a polydisperse discrete distribution. Fig. 6 [64] shows a comparison between experimental data on ternary mixtures [73,75,78] and model predictions. Initial porosities were chosen so that they can reflect different experimental conditions.

This approach can also be used to find the maximum packing fraction for a given mixture using

$$\begin{split} \phi_{max} &= max \left\{ \frac{1}{V_{max}} \right\} \\ &= max \left\{ \frac{1}{\sum_{i}^{n} V_{i} X_{i} + \sum_{1 \leq i \leq i}^{n} \beta_{ij} X_{i} X_{j} + \sum_{1 \leq i \leq j}^{n} \gamma_{ij} X_{i} X_{j} (X_{i} - X_{j})} \right\} \end{split}$$
(17)

subjected to the constraints $\sum_{i=1}^n X_i = 1$ and $X_i \geq 0$. However, the assumption that there are no higher-order joint actions shows obvious limitations when this model is used to find the maximum packing density for multi-component mixtures. As shown in Fig. 7 [64], for large ρ the predicted maximum packing density is greater than unity, which is obviously not physically possible. While one might consider that this relatively simple discrete model might be able to estimate packing densities for continuous distribution by binning the distribution into a discrete one with a large number of components, this limitation at high n makes such an approach impossible. Instead, a different method must be used, as described in the following section. However, for ternary mixtures this approach still provides useful estimates of the packing density.

4. Continuous distributions

As noted in the previous discussion, interactions between different particle sizes are substantial and do not decrease as more various sizes are added to a mixture. However, the particle systems encountered in practical applications are never monodisperse or discrete, but rather are characterized by continuous distributions of sizes. Such size distributions can be measured using various techniques, such as particle imaging. Systems are available that aerosolize particles in a jet of air and pass them in front of a pulsed laser illuminated camera system. The projection of the particle is captured and calibrated to the particle size [79,80]. These systems are able to individually image a substantial fraction of the particles in a sample, measuring millions of particles from a tablespoon-size amount of fine powder. In addition to size

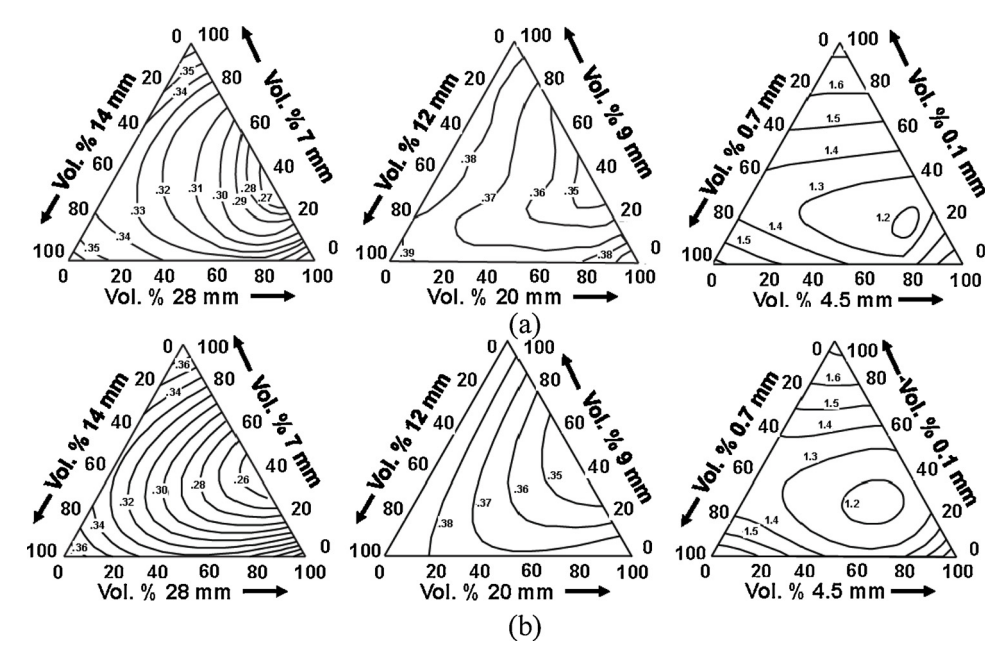


Fig. 6. Comparison of (a) experimental and (b) analytical predictions for ternary mixtures of three compositions. The figure is reused with permission from [64].

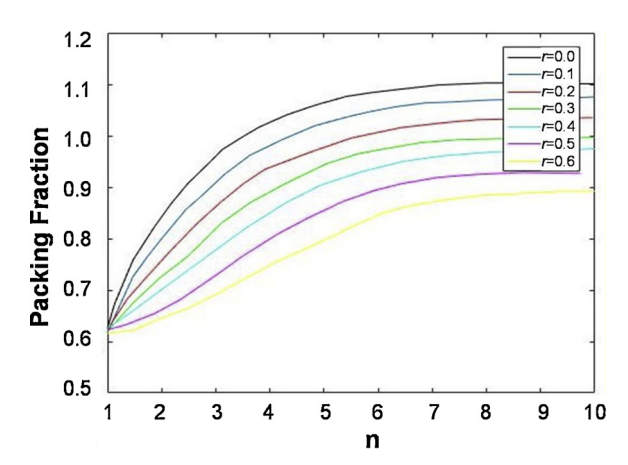


Fig. 7. Predicted maximum packing fraction as a function of number of components. The numbers next to the lines indicate ρ^{-1} . The figure is reused with permission from [64].

information these systems also provide shape distributions. Laser diffraction based systems are also available for accurate size measurement of sub-micron size particles with the same throughput.

A number of common distribution functions are used to model the experimentally measured size distributions. For instance, the Gaussian distribution is determined by its mean \bar{R} and standard deviation σ

$$f(R) = \frac{1}{\sigma\sqrt{2\pi}}e^{-\frac{(R-R)^2}{2\sigma^2}}$$
(18)

The log-normal distribution is a variation on the Gaussian, but over a logarithmically scaled variable

$$f(R) = \frac{1}{\log \sigma_g \sqrt{2\pi}} e^{-\frac{(\log R - \log R)^2}{2\log^2 \sigma_g}}$$
(19)

where σ_g is referred to as the geometric standard deviation.

Unfortunately, analytical treatment of continuous particle size distributions is not possible, so there is no simple bridge between the discrete systems discussed in the preceding sections and the discussion in the present section. In this section, various experimental results on packing of particles with continuous size distributions will first be

discussed, to give a sense of how these packings vary from the discrete systems discussed earlier. Then, various empirical relationships between properties of the distribution and the packing properties will be shown. These relationships are derived in terms of various mathematical properties of the distribution functions and provide a good framework for predicting packing properties of widely varied particle mixtures. The distribution properties, namely the moments, are simple to compute numerically for experimental particle size measurements.

4.1. Empirical results

One of the first systematic experimental studies on continuous size distributions was carried out by Sohn et al. who assessed mono-modal and bimodal Gaussian and log-normal distributions by weight (if the density of sand is assumed to be constant and independent of particle size, then the size distribution by volume and that by weight are identical) of two types of sand [81]. Dense random packing was ensured by tapping on the cylindrical container after pouring of the mixtures.

For Gaussian distributions, packing density was seen to increase continuously as the dimensionless standard deviation (σ/\bar{R}) increased. The increase in packing density obtainable by increasing the width of the distribution is considerable: a 23.3 % increase was achieved for $\sigma/\bar{R}=2/3$ with respect to uniform particles of the same mean size. While there is some scatter in the experimental data, the results indicate, as expected, that the mean particle size does not significantly affect the packing density.

Results for log-normal distributions are similar to the ones for Gaussian distributions: packing density increases continuously with increasing spread of size distribution. The highest value was obtained at $\sigma_g=6$, with an increase of 33.1 % with respect to uniform particles ($\sigma_g=1$) of the same sand at the same mean size. Again, the scatter of the data is relatively small showing that packing density is a function of size distribution only and is independent of mean particle size.

The bimodal systems examined were made up of either two Gaussian systems, or two log-normal systems, of different mean size but the same dimensionless standard deviation. Results plotted in Fig. 8 show that as the amount of larger mean-sized component is increased, the packing density increases up to a maximum at a composition of 55%–75% of larger component, while further increase in the amount of larger component decreases the packing density. This is much the same result as was observed in Fig. 3 for binary discrete mixtures.

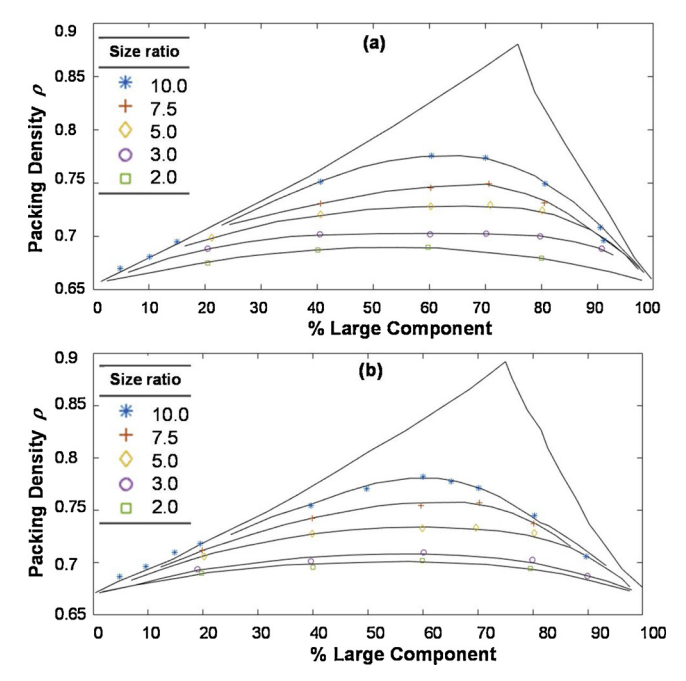


Fig. 8. Variation of packing density with mean-ratio and composition for binary mixtures of two (left) Gaussian and (right) log-normal systems (the uppermost curve represents $\rho \to \infty$). The figure is reused with permission from [81].

The highest packing densities obtained in these experiments for binary mixtures were 0.775 for Gaussian and 0.782 for log-normal, compared with 0.655 and 0.671 for the single distributions, and 0.570 to 0.607 for uniformly sized particles. The difference between the packing densities for the two distributions is generally small with log-normal systems having somewhat higher packing densities than Gaussian systems. This is due to the greater number of fine particles in the log-normal systems.

Packing density of a bimodal mixture depends upon both the increase obtained in forming the binary and upon the packing density of the individual components. Therefore, the packing density increase is less for continuous distribution systems than for discrete-sized systems because the packing density of the former has already been increased markedly in the individual components, compared to uniform-sized systems, before making up the binary mixture.

The linear analytical model presented earlier for the discrete case, developed by Yu et al. [74] and calibrated based on experimental results for binary mixtures, obtained good agreement for continuous distributions as well [81] as depicted in Fig. 9. One explanation for the error, apart from the lack of higher order interactions, is that the sand particles were not perfectly spherical.

4.2. Modeling

Models that use properties of the distribution function to predict the packing of a particle system are of obvious utility, since using modern equipment it is possible to characterize the distribution function relatively easily. Such models consider the moments of the distribution function. The k-th moment M_k of a distribution is defined as

$$M_k = \int_0^\infty R^k f(R) dR \tag{20}$$

and the moment of the modified distribution $\Delta R = R - \bar{R}$ is

$$\Delta M_k = \int_0^\infty \Delta R^k f(R) dR \tag{21}$$

Santos et al. used a statistical physics model based on the free energy of a hard sphere mixture in a spatially uniform equilibrium state, similar to a fluid at a constant pressure [82]. This analogy is not exactly

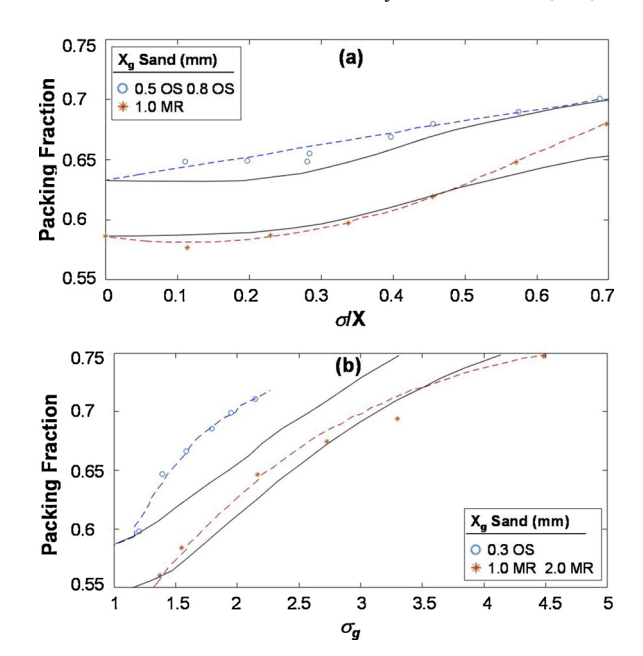


Fig. 9. Calculated porosity [74] (solid line) and experimental data (dashed line). The figure is reused with permission from [74].

applicable because the particle packings are far more (spatially) dense than typical gases. However, by assuming the model to still be valid near the jamming point of the mixture, useful results can be obtained. A jammed packing is defined as a particle configuration in which each sphere is in contact with its nearest neighbors so that mechanical stability is conferred to the packing.

A monodisperse system jams at the random close-packing density $\phi_{rcp} \approx 0.63$; as a consequence of their ability to attain higher packing fractions, the jamming packing fraction ϕ_T of a polydisperse system is typically higher than the random close-packing fraction.

A simple relationship was found between the jamming packing fraction and a single dispersity parameter $\boldsymbol{\lambda}$

$$\lambda = \frac{m_3}{m_2^2}$$
, where $m_k = \frac{M_k}{M_1^k}$ (22)

where the m_k are called the dimensionless reduced moments. The occupied-to-void volume ratio at jamming, $\phi_J/(1-\phi_J)$, is simply proportional to the one-component value $\phi_{rep}/(1-\phi_{rep})$ with λ as the coefficient.

$$\frac{\phi_J}{1 - \phi_J} = \lambda \frac{\phi_{rcp}}{1 - \phi_{rcp}} \tag{23}$$

The model in Equation above was compared against experimental and simulation data of binary, inverse power, and log-normal distributions, and accurately predicts the jamming (i.e. maximum packing) behavior within the range $1 \le \lambda \le 3$. The comparison with experimental results is shown in Fig. 10. It is interesting to note that $\sqrt{\lambda} = \sqrt{M_1 M_3}/M_2$ represents the ratio of the geometric mean of the average diameter and average volume of the spheres to their average area, giving the statistical parameter a geometric interpretation.

Desmond et al. [83] studied the effect of size distributions on maximum packing volume fraction using different continuous distributions: linear, Gaussian, and log-normal, all with the same mean size $\bar{R}=1$. To avoid negative radii, the Gaussian and log-normal distributions were truncated at R=0.1. The maximum packing fraction ϕ_{max} was mostly dependent on two parameters, the polydispersity δ and skewness S, defined below, and no substantial influence ($\leq 0.2\%$) of the kurtosis (a combination of higher order moments) was found.

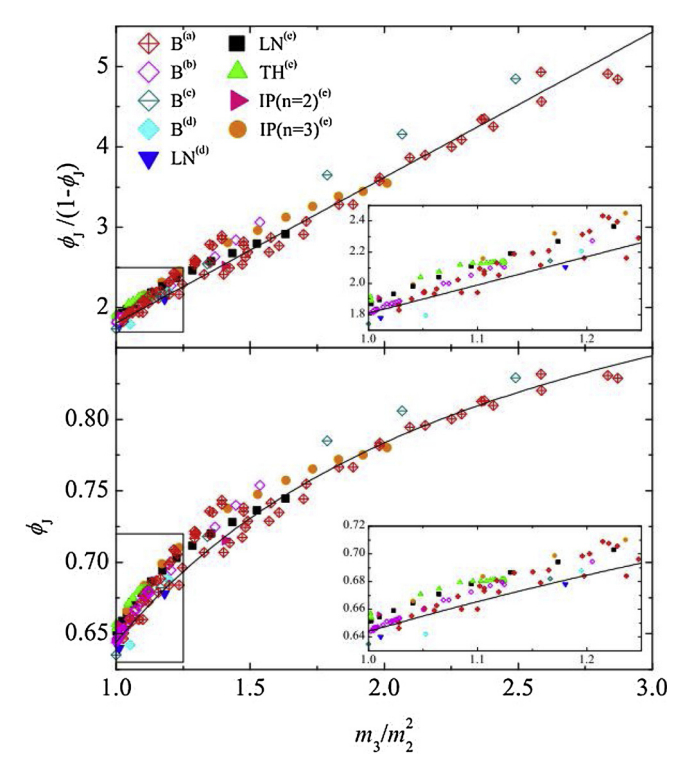


Fig. 10. Prediction of jamming packing fraction from a statistical mechanics approach [82].

$$\delta = \frac{\sqrt{\Delta M_2}}{M_1} \text{ and } S = \frac{\Delta M_3}{\Delta M_2^{3/2}}$$
 (24)

Based on experimental data, it was found that the relationship could be modeled with the form

$$\phi_{max} = \phi_{rcp}^* + c_1 \delta + c_2 S \delta \tag{25}$$

where $\phi_{rcp}^*=0.634$ is the packing fraction for a monodisperse packing of spheres ($\delta=0$ and S=0), and c_1 and c_2 are empirical constants, which were found to be $c_1=0.0658$, and $c_2=0.0857$. Comparison between the calibrated model predictions and experimental results for the different distributions is shown in Fig. 11. It was shown that increasing δ increases ϕ_{rcp} , and that, for a given δ , ϕ_{rcp} increases linearly with increasing S. As S can be negative, a negatively skewed f(R) can decrease ϕ_{max} as compared to a symmetric distribution. Two significant conclusions can be drawn from this work. First, the skewness has a significant influence on ϕ_{max} for distributions with large polydispersity. Second, Eq. 9 allows one to determine ϕ_{max} from only δ and S, without taking into account any other details of the shape of the distribution f(R). This empirical approach has also yielded more accurate predictions (\pm 0.2%)

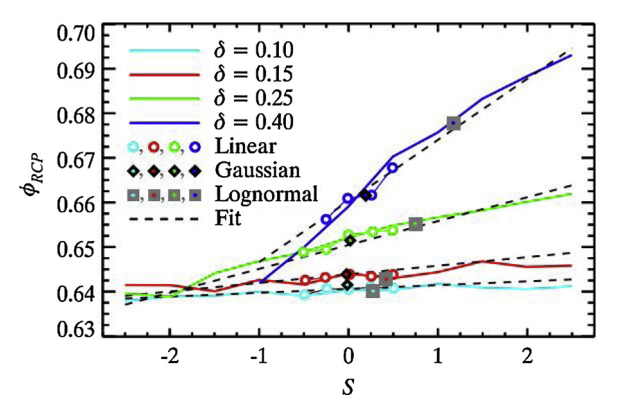


Fig. 11. Prediction of maximum packing fraction from Eq. 9 [83].

than the model based on statistical physics Eq. 23 which predicted the random close-packing fraction to within \pm 2%.

5. Non-spherical particles

So far, the discussion has been limited to spherical particles; naturally, the majority of particles encountered in the real world will not be perfectly spherical. In many cases, such as reused SLS powder that has been compacted previously, the shapes may be spheroidal. Further, depending on the powder production method, particles may be highly irregular. Non-spherical particle packings may also jam at densities much lower than their maximally dense configuration, making it difficult to apply methods such as the initial-porosity models or the interaction models.

In their experiments, Sohn et al. [81] noted that, for uniform sand particles and narrow size distributions, the packing density is greater for particles of higher sphericity. However, packing density increases more rapidly for the lower sphericity particles with the result that the higher sphericity particles tend to lose their comparatively advantageous packing character as the size distribution width is increased.

As in the section on continuous distributions, the complexity of the topic will limit the discussion here to the presentation of qualitative models, followed by experimental and simulation results. For uniformly sized particles, it is well-established that porosity generally increases with the decrease of sphericity, which is defined as the ratio of the surface areas between a sphere and a particle of the same volume. Non-spherical particles such as sphero-cylinders, ellipsoids and spheroids exhibit very similar packing behavior, consistent with their similarity in shape, with respect to the maximum density for near-spherical shape, and the density decrease at higher aspect ratios. A slight deviation from spheres by the use of cutting, elongating or deforming spheres still forms disordered packings with similar structure to random sphere packings.

5.1. Equivalent packing size model

An analogy to the spherical particle linear model can be made when considering convex particles, which includes both particle size and shape [84]. These models involve a property known as the "equivalent packing diameter," which is essentially a modified diameter that accounts for the differences in packing caused by the shape effect. The equivalent packing diameter of a component is determined by measuring a size-dependent packing property and finding the diameter of a sphere having the same magnitude of the property (for example, the equivalent packing diameter of cylindrical particles has been investigated in [85]). The porosity of a particulate system, ε , can generally be expressed as a function of volume fractions X_i , equivalent packing diameter d_{pi} and initial porosity ε_i of its components:

$$\varepsilon = f(X_1, ..., X_n, d_{p1}, ..., d_{pn}, \varepsilon_1, ..., \varepsilon_n)$$
(26)

According to this modified linear packing model, the specific volume of the mixture, *V*, defined as the reciprocal of the packing density, can be determined by the following equation:

$$\frac{1}{1-\varepsilon} = V = \max\{V_1^T, \ldots, V_n^T\}$$
(27)

where

$$V_i^T = \sum_{j=1}^{i-1} \left[V_j - (V_j - 1)g(r_{ij}) \right] X_j + V_i X_i + \sum_{j=1}^{i-1} \left[1 - f(r_{ij}) \right] X_j$$
(28)

in which V_i are the specific volumes of the individual components of the mixture which can be determined from their initial porosity ε_i . The interaction functions $f(v_{ij})$ and $g(v_{ij})$ have been fitted to experimental data of binary mixtures and are only dependent on the (small-to-large) ratio of the diameters between components i and j.

$$f(r_{ij}) = (1 - r_{ij})^{3.33} + 2.81r_{ij}(1 - r_{ij})^{2.77}$$

$$g(r_{ij}) = (1 - r_{ij})^{1.97} + 0.36r_{ij}(1 - r_{ij})^{3.67}$$
(29)

The dependence on particle shape is eliminated, provided that the size-ratio r_{ij} is evaluated in terms of equivalent packing diameter. Eq. 29 can be satisfactorily used in the porosity estimation of non-spherical particle mixtures and also to the packing of fine particles (typically smaller than 100 µm) [86].

5.2. Computational simulations

Computational studies have allowed studying parameters that are difficult to model in theory. For example, mixtures of particles of different length scales, shapes, and surface properties have been simulated to develop an understanding about their packing behavior. Simulations with the mechanical contraction method (MCM) performed by Williams et al. [87] showed that the volume fractions of long sphero-cylinders (thin rods with spherical caps) is inversely proportional to the aspect ratio α . The maximum packing density of spheres, $\alpha = 0$, was shown to be a local minimum: the highest density $\phi = 0.70$ occurs at $\alpha = 0.4$, as shown in Fig. 12. The practical implication is that a small deviation in shape from spherical may increase the random packing density significantly. Studies on packed bed characteristics are also available in the context of flow through porous media. Simulations and modeling studies have focused on determining the flow characteristics in the packed porous beds [88,89]. Flow of gases in the thick packed beds may represent a similar problem and can benefit from these studies. In these studies, a property called tortuosity is defined as the degree of deformation of flow paths within the medium. Tortuosity is found to be dependent on the packing factor as well as particle shape. Beds of simpler particle shapes such as spheres could be modeled theoretically [89]. Packed beds of various particle morphologies such as tubes and rings have been studied for packing and porosity characters but experimental validation of such results is difficult because the beds of exact same characteristics cannot be created [88].

Donev et al. [90] found through experiments and computer simulations that for spheroids and ellipsoids, both the average coordination number and random packing density increase rapidly as the particles slightly deviate from perfect spheres (Fig. 13). Remarkably high densities for uniform size particles, such as $\phi = 0.71$ for spheroids, and $\phi = 0.735$ for ellipsoids were found, approaching the highest possible

density of face-centered cubic or hexagonal close-packed crystals. This work suggested that the denser random packing of non-spherical particles is related to the rotational degrees of freedom per particle introduced by lack of symmetry and thus the larger number of particle contacts required to mechanically stabilize the packing, as forming more contacts requires a denser packing. For very aspherical particles it is not possible to align themselves due to entanglement and jamming, therefore the excluded volume effects start to dominate and the packing density decreases. Simulations on the variation in the aspect ratio of spheroidal particles showed that the aspect ratios of 0.6 and 1.8 resulted in densest packed beds for oblate and prolate spheroid shapes. respectively [91]. Simulations of bed heating showed that ellipsoids have lower convective heat transfer rate but higher conductive heat transfer rate than spherical particles [92]. Further, in fluidized beds, the convective heat transfer coefficients of prolate particles are larger than those of spheres and oblate particles [92].

Further MCM computer simulations were carried out by Wouterse et al. [93] to investigate the effect of particle shape and aspect ratio on packing density of cut spheres (a spherical segment which is symmetric about the center of the sphere). It was found that cut spheres, similar to sphero-cylinders and spheroids, pack more efficiently as the aspect ratio is perturbed slightly from unity (the aspect ratio of a sphere), reaching a maximum density at an aspect ratio of approximately 1.25. Upon increasing the aspect ratio further, the cut spheres pack less efficiently. The results for percolations of particles of various shapes through the packed bed are interesting [94]. Discrete element method is used to simulate the percolation behavior and the results show that both spherical and cubical particles have a constant velocity during percolation through packed bed but cubical particles are found to have greater percolation velocity [94].

For higher aspect ratios the packing behavior of cut spheres and sphero-cylinders is very different from that of spheres and also dependent on simulation parameters because of the existence of planar faces, or a strongly dominant dimension of the particle creating strong exclusion-volume effects.

One of the major limitations of simulation studies on packed beds is that the exact structure of the bed simulated in the model cannot be generated for experiments to validate the results. Therefore, most studies develop theoretical bounds for the behavior of packed beds. As an innovative application, AM technologies have been used in this field to conduct experimental validation of simulation results obtained for tortuosity in packed beds by fabricating beds of different characters

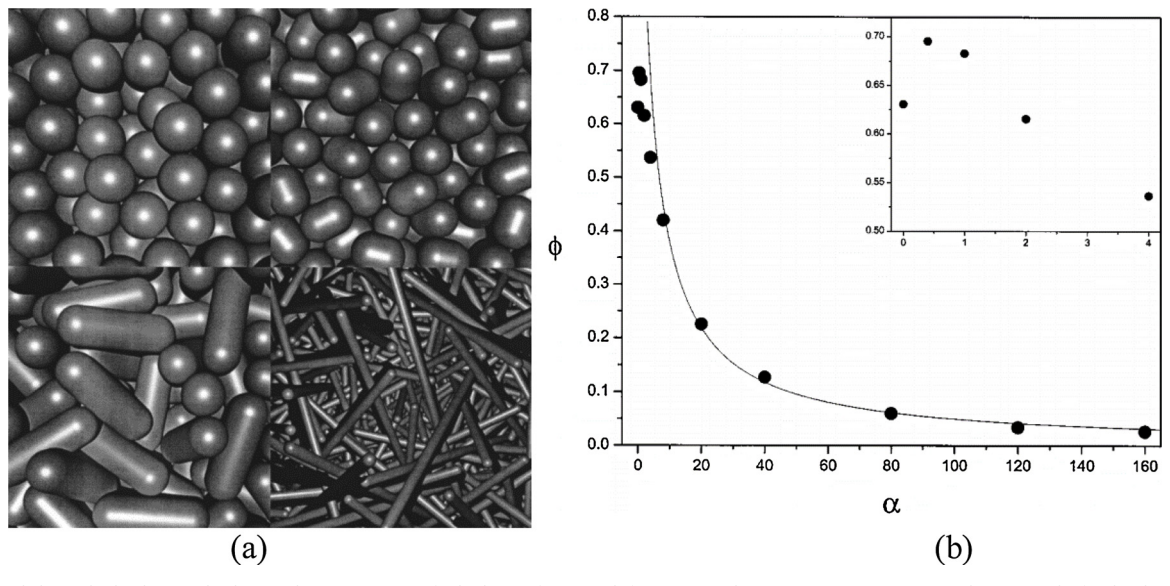


Fig. 12. (a) Tightly packed sphero-cylinders with aspect ratios of (clockwise from top left) $\alpha = 0$ (spheres), $\alpha = 0.40$, $\alpha = 40$, and $\alpha = 2.0$; (b) final volume fractions ϕ as a function of aspect ratio α [87].

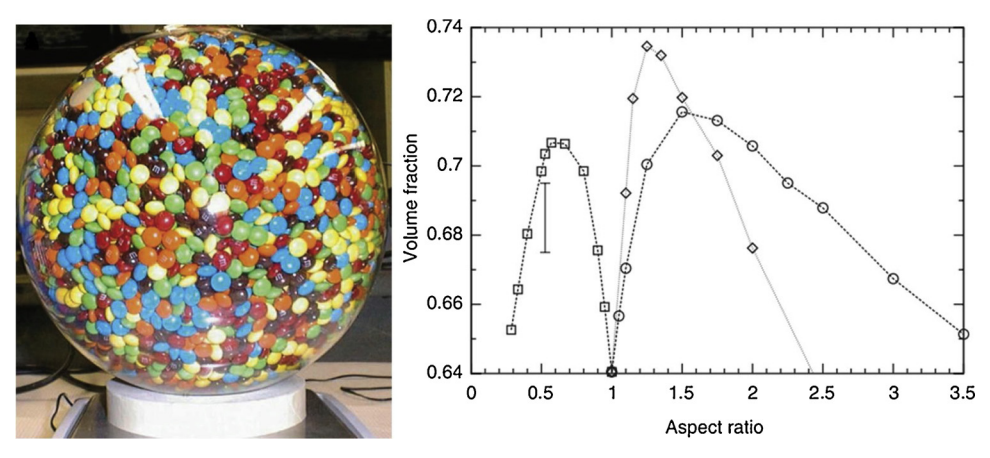


Fig. 13. (a) An experimental packing of ellipsoidal candies and simulated final volume fractions ϕ as a function of aspect ratio α [90]. The bar at AR = 0.5 shows the range of values obtained by experiments.

exactly as represented in the simulation studies [95].

6. Considerations for fine particles

In earlier sections which dealt with purely geometric considerations in the packing of particles, it was shown that the packing properties are not affected by the absolute magnitude of the particle sizes, but rather only their sizes relative to one another. However, it is often observed in experiments that "small" particles tend to randomly pack to lower densities than larger ones. This effect can be observed, for instance, with tungsten and aluminum particles sieved through a 40 µm opening. Though these particles are nearly spherical and have smooth surfaces, their random packing density is significantly less than that of round steel shot of the same size [54]. Nanoscale packed beds have been studied for thermal conductivity characteristics. The thermal resistance between nanoparticles is found to increase with a decrease in the particle contact radius [96]. While highly packed beds are desirable for additive manufacturing to minimize the void volume fraction in the bed, reduced thermal conductivity can be a limitation in using nanoscale particle beds. Forces associated with agglomeration begin to contribute and work to oppose systematic packing: the micron-scale powder packs poorly by itself and could be so agglomerated that it behaves as a larger, rough particle. This observation is especially relevant to packed particle beds used in AM because several methods used particles in the size range that is affected by such effects. Self-assembly of nanoparticles has been studied widely to understand the effect of particle size, shape and crystal growth kinetics on the density of the assemblies [97]. This study finds that the final shape of the assembly is not the optimal shape predicted by thermodynamics but small entropy contributions from shape imperfections may contribute significantly

When particle size is smaller than a threshold value, gravity no longer dominates, and inter-particle forces, such as van der Waals and electrostatic forces 4 , become more important. When particle diameter is less than 100 μm , the ratio of inter-particle force to the weight of particles is greater than unity [98]. This causes formation of aggregates or agglomerates because of the relatively strong cohesive forces. As a consequence, the particles do not behave individually at the macroscopic level.

Due to the large number of relevant factors in approaching this problem, wide systematic studies are difficult; most of the literature available is limited to certain cases or material systems. A computer simulation of random evolution of spherical particles has been performed by Yen at al [99]: about 1000 monosized particles were loosely placed inside a rigid cylindrical container and allowed to settle under gravity. Van der Waals interactions (VDWI), frictional forces, and Hertz contact forces were included, and particle size was kept constant at 100 μm. When only gravity was considered (case I), packing density reached an average steady value of 0.633, close to a random close-packed structure. When a frictional coefficient of 0.3 was introduced (case II), packing density reached a steady value of only 0.578. When VDWI was introduced in addition to friction (case III), the steady-state density reached only 0.528. When, in addition to VDWI, the friction coefficient was increased to 0.7 (case IV), the steady-state density was 0.505. Finally, for 50 µm particles (case V), with VDWI and friction coefficient of 0.3, the packing density reached only 0.420 as gravity could not cause enough rearrangement by breaking the clusters formed due to the VDWI.

Yu et al. [86] have successfully modeled this phenomenon by use of the initial porosity of mono-sized particles and the concept of equivalent packing size-ratio as a measure of the particle-particle interaction in forming a packing of mixed powders. This model was experimentally validated for white fused alumina powder.

These phenomena generally occur for particle size on the order of 100 μ m. Beyond this threshold, porosity increases with decreasing particle size. General assessment of this relationship is difficult, and even more so when the effect of particle shape and its interaction with particle size is considered. Therefore, to evaluate the cooperative packing behavior, the relationship between porosity ε_d and (median) particle size d has to be established experimentally as well as the relationship between equivalent packing size-ratio, r_{ij} and initial (median) ratio of small-to-large components R_{ij} , in order to compute the values to be used in Eq. 28 to calculate the porosity of the mixture.

One important feature is that the equivalent packing size-ratio is always greater than its corresponding initial ratio. Noting that the packing size-ratio is a measure of the interaction between two components, the fine particles do not simply fill in the void among large particles but may stick on their surface and form heterogeneous agglomerates. The larger the difference in particle sizes, the more significant is this behavior and the increase in final porosity. For the eleven alumina powders, it appears that these results can be well represented by the equations

$$\varepsilon_d = \varepsilon_0 + (1 - \varepsilon_0)^{-ad^b}$$

$$r_{ij} = R_{ij}^p$$
(30)

where ε_0 , a, b and p are fitting parameters.

This approach should be applicable to the packing of other fine

 $^{^4}$ For electrically insulating particles, the electrostatic forces can dominate even at larger scales. This is best observed when breaking apart a piece of expanded polystyrene packing material (Styrofoam) – the beads (${\approx}5 \mathrm{mm}$ diameter) repel strongly and can attach to the walls of the box.

particulates where an accurate predictive method is required, probably with modified equations for evaluating the initial porosity and packing size-ratio.

7. Implications for additive manufacturing

Metal additive manufacturing processes like Selective Laser Sintering (SLS), Selective Laser Melting (SLM) and binder jetting use metal powder as raw material, as such the consistency of the powder has a strong influence on the final component properties. Different processes may be affected by the same parameters to a different degree. A discrete amount of powder is mechanically spread across the build plate to form a thin layer of powder in SLM and SLS processes. It is critical that the layer is homogenous over the entire area of the build chamber, any degree of inhomogeneity may result in porosity or incomplete through-thickness melting. The layer spreading, hopper dosing and bulk packing performance of the AM powder will depend on the properties of the powder being used. Recent studies have closely looked at the characteristics of a single layer spread on the build plate [100]. The packing density in a single layer in SLM process is found to be much lower than estimated by common theoretical methods [100]. Numerical studies determined substantially lower packing densities than expected as observed in Fig. 14. A packing density of 20 and 38 % in layer heights of 30 µm and 50 µm, respectively, was observed for a powder with a particle size distribution between 15 and 75 µm and a tap density of over 50 % [101]. Reduction in the actual bed density occurs for many reasons, including that the surface of the previously solidified layer is lower than expected due to filling of pores by the molten metal, sputtering and vaporization.

Further complicating the use of powder is that the volume of the actual component built can be significantly less than the total volume of powder that has been spread. As a consequence, there is a large amount of unused powder left over in the build chamber, given the high cost of metal powders it is essential that the unused powder is effectively recovered and reused in future builds [102]. The effects that result from the thermal cyclic process cause physical as well as chemical changes to the recycled powder and depend on the powder metal [103]. Observations on steel powder showed that there was an increase from 27 to 34 % in the oxygen content of the recycled powder, whereas Fe and Mn contents decreased. Overall, the changes were not expected to drastically change the powder properties. It has been observed that recycling a nickel-based superalloy powder results in a marginal decrease in mean particle size without changing the shape of the distribution [104]; whereas after twelve cycles, the average size of a Ti-6Al-4 V alloy powder increased from 37.4-51.2 μm (36.8 %) and the size distribution is enlarged as a consequence of partial sintering because of residual heat close to the melt pool [105].

7.1. Metal powder production

The production of AM metal powder generally consists of three major stages: the first stage involves the mining and extracting of ore to form a pure or alloyed metal product (ingot, billet and wire) appropriate for powder production; the second stage is powder production and the final stage is classification and validation. Morphologies of powders produced by various methods are compared in Fig. 15.

Atomization has been identified as the best way to form metal powders for AM due to the geometrical properties of the powder it yields; nevertheless, a minimum post processing is necessary: the as-produced metal powder is sieved into a particle size range suitable for the required process: typically 15–45 μm for SLS/SLM and 45–106 μm for electron beam melting [106].

Inert gas (Nitrogen, Helium or Argon) atomization with melting under vacuum is the leading powder production process for a variety of high-grade metal powders like titanium alloys, steels, aluminum alloys nickel-based superalloys. Gas atomization is a widespread method because powders can achieve spherical shape, rapid solidification, homogeneous microstructure and good packing. However, gas atomized powders are only nominally spherical as the presence of smaller satellites agglomerating on coarser particles is frequent [104,107,108].

Another production process is carried out by impinging a falling stream of molten metal with jets of water which immediately solidify the metal into granules or powder. Water atomization presents a cost effective and efficient approach to producing metallic powders. On the other hand, irregular angular particle shape due to the rapid quench, lower tap densities and oxidized surfaces persist in this method. Asproduced powder size can be further reduce reduced by conventional ball milling resulting in a less irregular in shape. A new method of water atomization using high pressure and flow rate has been used to produce a very fine silver powder of spherical, elliptical, and irregular morphology and a very low oxygen content [109].

In centrifugal atomization, the centrifugal force from a rotating disk breaks up the molten metal and sprays off droplets that then solidify as powder particles. This method is more energy efficient than gas and water atomization but cannot produce powder of size much below 100 μ m. During "Rotating Consumable Electrode Atomization" the end of a metal bar is melted by plasma while it is rotated about its longitudinal axis. Molten metal is centrifugally ejected and forms droplets that solidify to spherical powder particles. Despite of its higher cost and the limited suppliers, this method has many advantages such as almost perfect sphericity and absence of agglomeration or contamination. Powders are very free flowing and hence have a high packing density.

The quality of a component built in an AM process is assessed based on part density, dimensional accuracy, surface finish, build rate and mechanical properties. To achieve predictable and consistent component quality, it is desirable that the characteristics of the powder bed, such as temperature and density, are maintained at a constant level. These characteristics are governed by some powder process variables.

Particle morphology will have a significant impact on the bulk packing and flow properties of a powder batch. Research into the effect of particle morphology on the AM process has shown that morphology can have a significant influence on the powder bed packing density and consequently on the final component density, where the more irregular the particle morphology the lower the final density. As a consequence of this, highly spherical particles tend to be favored in the AM process.

Particle size distribution will also have an impact on minimum layer thickness and geometric resolution of the component. From the combination of microscopy and granulometric analysis, the AL–Si-Mg powders employed in the study was made of a large amount of very small spheres and only a few bigger ones. Finer particles provide a larger surface area to absorb more laser energy, leading to a faster sintering rate. However, very fine particles with a diameter less than 10

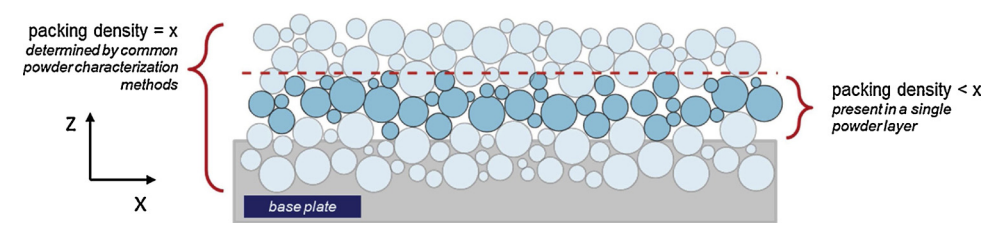


Fig. 14. Packing density of powder in a single layer on build plate in SLM [100].

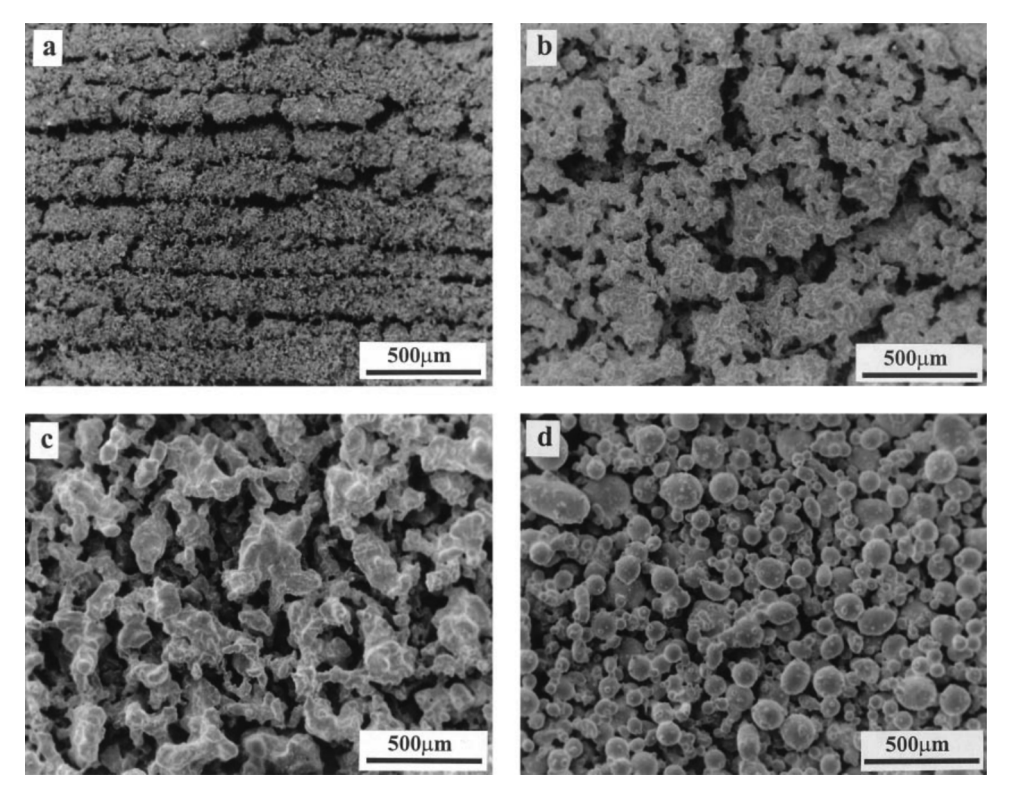


Fig. 15. SEM images of steel powders showing the shape of particles (a) ball milled ($\bar{D} = 11 \mu m$); (b) water atomized ($\bar{D} = 32 \mu m$); (c) water atomized ($\bar{D} = 100 \mu m$); (d) gas atomized ($\bar{D} = 117 \mu m$) [107].

µm tend to agglomerate, forming bigger clusters of irregular shape which adversely affect the flowability of the powder and the layer density: it is fundamental to sieve the powder to ensure a maximum particle size in agreement with the layer thickness when filling the machine [108]. However, when the powder particles are very coarse and the particle size distribution is broad, the bed density is less than the tap density, meaning that, for an inappropriate layer thickness, mechanical recoating is likely to cause powder segregation and/or agglomeration [110].

Generally, it is well reported that a high fine content distribution produce components with a higher fractional density [111]. However, the use of fine materials increases the risk of health and safety issues. This is particularly true when processing reactive materials such as titanium where finer particulates are likely to be more flammable and explosive.

7.2. The effect of particle size distribution on AM process and part quality

A study about the influence of particle size distribution on the quality of the final part has been proposed by [107]. In this work, three different sizes of gas atomized, water atomized and ball milled high-speed steel (HSS) powders were laser-sintered to understand the effect of the particle size and morphology on sinterability. Angular shaped water atomized powder particles have a higher surface area per unit volume and therefore they can absorb more laser energy, leading to an enhanced sintering process. However, non-spherical particles give a lower random packing density and coordination number than spherical particles. This limits the densification process and results in the formation of agglomerates and pores, or segregate toward the center of laser beam, as found in laser sintered water atomized powder. These phenomena are believed to be caused from a combination of irregular shape and high oxygen content in the powder particles. SLS of gas atomized powder results in the formation of a homogeneous and dense layer.

Studies on binder jetting process are also available to document the

impact of particle size, size distribution and shape on the printed part quality. Imaging techniques are now widely used for observing dynamic effects of these parameters on the print quality [112]. A review article is available that summarizes many of these effects in detail [113]. Similar to the SLM and SLS processes, the wider particle size distribution is found to provide higher packing. However, binder jetting process is usually followed by a sintering step. A narrow particle size distribution is favored to obtain better flow characteristics, a wider size distribution is preferred to make the part more dimensionally and structurally stable during sintering step. Smaller particle feed materials provided better surface finish, dimensional accuracy, and higher hardness in the sintered part [114].

In [110], a close relationship between the densification, the processing parameters and the powder characteristics is demonstrated. Iron powders produced by water atomization or a thermal decomposition process known as carbonyl process, and gas-atomized prealloyed powders of 316 L stainless steel and M2 high-speed steel were laser sintered. Sieving was used to obtain different particle sizes ranging from 10 to 200 μm . The carbonyl and gas atomized powders have near spherical shape while the water-atomized iron powders have irregular particles.

Laser power (P), scan rate (ν), scan line spacing (h), and thickness of layer (d) are the main factors influencing the densification kinetics. The scanning geometry, working atmosphere, and powder bed temperature are also effective, although to a lesser extent. Since several factors influence the sintered density, it would be helpful if a single factor were introduced. Based on the energy conservation rule, the factor can be expressed as $\Psi = P/vdh$, representing the total energy input per volume of each sintered track. The fractional density (ρ)-energy input (Ψ) curves for the investigated iron powders are shown in Fig. 16 and are fitted to the following model:

$$\rho = C_1 - C_2 \exp(-K\Psi) \tag{31}$$

The results show that the sintered density increased sharply with increasing the specific energy input, according to the densification

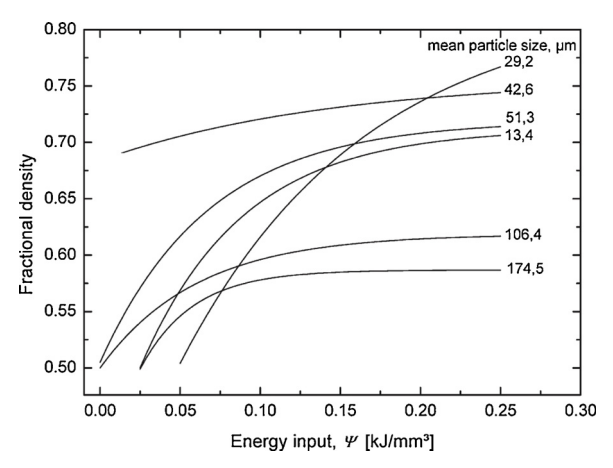


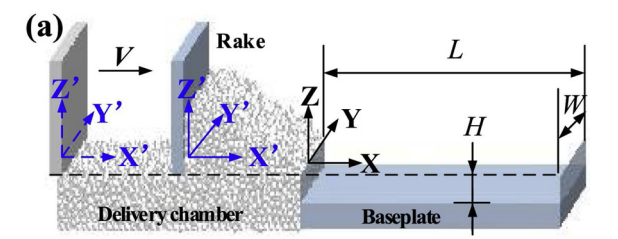
Fig. 16. Fractional density vs specific energy input for the investigated iron powders [110].

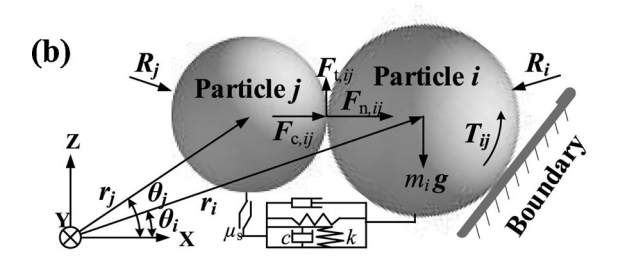
coefficient K, until a critical energy input was reached. The increase in the sintered density was followed with further increasing the specific energy, but at a slower rate. At an even higher energy input, the sintered density almost turns to remain constant, this constant is named "saturation density" ($\approx C_1$) and is always less than unity, meaning the powder material cannot be sintered to full density even at very intensive laser energy input. It has been found that at constant oxygen concentration, the K value increases and C_1 value decreases as mean particle size increases. In other words, if powders have the same characteristics with respect to particle shape and purity, coarser powders show lower densification in laser sintering.

In a different study [115], it was confirmed that the densification rate of finer powders is greater than the coarser ones. Furthermore, the effect of fabrication parameters was also considered: the effect of particle size is more pronounced at higher laser energy for a smaller layer thickness (50 μm); in contrast, at layer thickness of 200 μm the impact of powder particle size on the densification appears more noticeably at lower laser energy inputs.

Even when considering full melting of the powder in the SLM process, experiments confirm that a wider particle size distribution provides higher powder bed density; this generates higher density parts and smoother side surface finishing for a given energy input. A narrower particle size distribution provides better flowability; this generates parts with higher strength and hardness [116]. Studies on using different particle size distribution demonstrate that the size distribution has a remarkable effect on the quality of printed part and surface roughness can be controlled by means of particle size distribution [117]. The post processing of a part is time consuming and expensive. Adjustment of feed material parameter can provide part of desired quality and reduce the post-processing requirements. Simulation and experimental studies have also demonstrated that the light absorption in the particle bed depends on the porosity in the bed and is a function of the particle size distribution [118]. Since the RCP of same size spheres is ~ 0.64 , the reflections of the light beam from the substrate plays in important role in the beds of narrow particle size distributions. Increased packing obtained for bimodal particle systems allows greater interaction between particles and the laser beam and greater absorption by the bed, which is especially beneficial for reflective powders. Bimodal distribution is found to have at least twice the absorptivity compared to the Gaussian distribution in the same material type as determined by experimental and simulation studies on thin powder layers [119,120].

Much of the existing work has focused on the characteristics of packed beds. However, in AM processes, a packed bed is created in each layer and the total number of layers can be thousands in one part. In such case, the mechanism of bed creation for feed particles of different





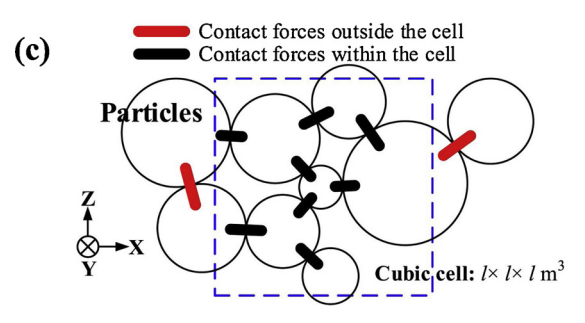


Fig. 17. Schematic of the discrete element method model: (a) powder-spreading process; (b) interaction forces between powder particles; and (c) stress within the powder system. In (c), the simulation zone is divided into virtual cubic cells of $l \times l \times l$ m³. The stress in a cubic cell is defined as the total contact forces per unit volume. The black bars denote the contact forces within the cubic cell and the red bars denote the contact forces outside [122] (For interpretation of the references to colour in this figure legend, the reader is referred to the web version of this article).

shapes, sizes and size distributions becomes important. Some studies are now available that focus on analyzing the characteristics of piles and bed formed by particles of different size distributions [121]. Fig. 17 shows the effect of feeding mechanism and powder particle size on the structure and properties of the packed bed simulated using discrete element methods [122]. An important finding in this work is the dynamic wall effect when the powder is being spread on the print bed, which results in lower density in thin powder beds. The thick powder beds result in 50–70 % packing but thinner beds have lower packing as observed by the simulation results and verified experimentally.

8. Summary and outlook

The interest in the AM field is expected to remain strong and even grow because of the possibilities of realizing structures that could not be manufactured with the traditional methods, individual product customization, and short development time scale due to rapid turnaround, among many other factors. Powder-based methods are also expected to continue to develop due to their versatility in developing complicated shapes without the use of a second support material. However, challenges related to powder bed methods are well documented and progress is being made to enable a) production of net shapes that do not require any post-processing, b) integrate heat treatments with the manufacturing methods, c) integrate quality

control with the manufacturing method, d) obtain high quality surface finish, and e) reuse the excess powder to reduce the total processing cost and wastage. Processing parameter optimization is an important step in developing an AM method for a given material, where laser power, spot size, sintering speed and other parameters are optimized. Powder characteristics are important for many of these considerations and are subjected to detailed studies. The packing of powder on the AM print bed is an important factor in determining the properties such as porosity in the bed, thermal conductivity of the bed, and thermal expansion due to heating. In the process of optimization of print parameters for a given material, repeatability in obtaining a given packing fraction is important. Even if the packed bed has less than closed packed particle arrangement, high quality parts can be obtained if the packing fraction is consistent from one layer to the other. The laser scanning speed and laser power can be optimized based on the packed bed density. Improved understanding of particle packing characteristics can help in selecting powders of characteristics that can provide beds resulting in high quality AM parts.

9. Declaration of Competing Interest

Authors declare no conflict of interest related to this work.

Acknowledgments

Author NG acknowledges U.S. National Science Foundation grant DGE-1931724 for partially supporting this work. Authors thank Keerthana Prakash and Xianbo Xu for help with preparation of some of the figures.

Appendix A. Supplementary data

Supplementary material related to this article can be found, in the online version, at doi:https://doi.org/10.1016/j.mtcomm.2020. 100964.

References

- D. Saltzman, M. Bichnevicius, S. Lynch, T.W. Simpson, E.W. Reutzel, C. Dickman, R. Martukanitz, Design and evaluation of an additively manufactured aircraft heat exchanger, Appl. Therm. Eng. 138 (2018) 254–263.
- [2] R. Huang, M. Riddle, D. Graziano, J. Warren, S. Das, S. Nimbalkar, J. Cresko, E. Masanet, Energy and emissions saving potential of additive manufacturing: the case of lightweight aircraft components, J. Clean. Prod. 135 (2016) 1559–1570.
- [3] M. Fateri, A. Kaouk, A. Cowley, S. Siarov, M.V. Palou, F.G. González, R. Marchant, S. Cristoforetti, M. Sperl, Feasibility study on additive manufacturing of recyclable objects for space applications, Addit. Manuf. (2018).
- [4] S.S. Gill, H. Arora, Jidesh, V. Sheth, On the development of Antenna feed array for space applications by additive manufacturing technique, Addit. Manuf. 17 (2017) 39–46
- [5] M. Javaid, A. Haleem, Additive manufacturing applications in medical cases: a literature based review, Alexandria J. Med. (2017).
- [6] E. Schwarzer, S. Holtzhausen, U. Scheithauer, C. Ortmann, T. Oberbach, T. Moritz, A. Michaelis, Process development for additive manufacturing of functionally graded alumina toughened zirconia components intended for medical implant application. J. Eur. Ceram. Soc. (2018).
- [7] S.E. Zeltmann, N. Gupta, N.G. Tsoutsos, M. Maniatakos, J. Rajendran, R. Karri, Manufacturing and security challenges in 3D printing, JOM 68 (7) (2016) 1872–1881.
- [8] ISO/ASTM 52900, 2015(En): Additive Manufacturing General Principles Terminology, (2015).
- [9] A. Mostafaei, P. Rodriguez De Vecchis, I. Nettleship, M. Chmielus, Effect of powder size distribution on densification and microstructural evolution of binder-jet 3Dprinted alloy 625. Mater. Des. 162 (2019) 375–383.
- [10] Y.S. Lee, P. Nandwana, W. Zhang, Dynamic simulation of powder packing structure for powder bed additive manufacturing, Int. J. Adv. Manuf. Technol. 96 (1) (2018) 1507–1520.
- [11] C.L.A. Leung, S. Marussi, R.C. Atwood, M. Towrie, P.J. Withers, P.D. Lee, *In situ X*-ray imaging of defect and molten pool dynamics in laser additive manufacturing, Nat. Commun. 9 (1) (2018) 1355.
- [12] M.N. Ahsan, R. Bradley, A.J. Pinkerton, Microcomputed tomography analysis of intralayer porosity generation in laser direct metal deposition and its causes, J. Laser Appl. 23 (2) (2011) 022009.
- [13] B. Song, T. Yu, X. Jiang, W. Xi, X. Lin, The relationship between convection mechanism and solidification structure of the iron-based molten pool in metal laser

- direct deposition, Int. J. Mech. Sci. 165 (2020) 105207.
- [14] A.T. Sidambe, Y. Tian, P.B. Prangnell, P. Fox, Effect of processing parameters on the densification, microstructure and crystallographic texture during the laser powder bed fusion of pure tungsten, Int. J. Refract. Metals Hard Mater. 78 (2019) 254-263
- [15] J. Delgado, J. Ciurana, C.A. Rodríguez, Influence of process parameters on part quality and mechanical properties for DMLS and SLM with iron-based materials, Int. J. Adv. Manuf. Technol. 60 (5) (2012) 601–610.
- [16] J.C. Fox, S.P. Moylan, B.M. Lane, Effect of process parameters on the surface roughness of overhanging structures in laser powder bed fusion additive manufacturing, Procedia Cirp 45 (2016) 131–134.
- [17] S.M.H. Hojjatzadeh, N.D. Parab, W. Yan, Q. Guo, L. Xiong, C. Zhao, M. Qu, L.I. Escano, X. Xiao, K. Fezzaa, W. Everhart, T. Sun, L. Chen, Pore elimination mechanisms during 3D printing of metals, Nat. Commun. 10 (1) (2019) 3088.
- [18] E. Olatunde Olakanmi, Laser sintering of blended Al-Si powders, Rapid Prototyp. J. 18 (2) (2012) 109–119.
- [19] C. Meier, R. Weissbach, J. Weinberg, W.A. Wall, A.J. Hart, Critical influences of particle size and adhesion on the powder layer uniformity in metal additive manufacturing, J. Mater. Process. Technol. 266 (2019) 484–501.
- [20] P. Wei, Fundamentals of radiation heat transfer in AlSi10Mg powder bed during selective laser melting, Rapid Prototyp. J. 25 (9) (2019) 1506–1515.
- [21] M. Marrey, E. Malekipour, H. El-Mounayri, E.J. Faierson, A framework for optimizing process parameters in powder bed fusion (PBF) process using artificial neural network (ANN), Procedia Manuf. 34 (2019) 505–515.
- [22] H. Masuo, Y. Tanaka, S. Morokoshi, H. Yagura, T. Uchida, Y. Yamamoto, Y. Murakami, Influence of defects, surface roughness and HIP on the fatigue strength of Ti-6Al-4V manufactured by additive manufacturing, Int. J. Fatigue 117 (2018) 163–179.
- [23] C. Chen, Y. Xie, X. Yan, S. Yin, H. Fukanuma, R. Huang, R. Zhao, J. Wang, Z. Ren, M. Liu, H. Liao, Effect of hot isostatic pressing (HIP) on microstructure and mechanical properties of Ti6Al4V alloy fabricated by cold spray additive manufacturing, Addit. Manuf. 27 (2019) 595–605.
- [24] A. Kumar, Y. Bai, A. Eklund, C.B. Williams, Effects of hot isostatic pressing on copper parts fabricated via binder jetting, Procedia Manuf. 10 (2017) 935–944.
- [25] L. Tan Phuc, M. Seita, A high-resolution and large field-of-view scanner for in-line characterization of powder bed defects during additive manufacturing, Mater. Des. 164 (2019) 107562.
- [26] L.C. Wei, L.E. Ehrlich, M.J. Powell-Palm, C. Montgomery, J. Beuth, J.A. Malen, Thermal conductivity of metal powders for powder bed additive manufacturing, Addit. Manuf. 21 (2018) 201–208.
- [27] A.V. Gusarov, E.P. Kovalev, Model of thermal conductivity in powder beds, Phys. Rev. B 80 (2) (2009) 024202.
- [28] S. Polesek-Karczewska, Effective thermal conductivity of packed beds of spheres in transient heat transfer. Heat Mass Transf. 39 (5) (2003) 375–380.
- [29] S. Zhang, B. Lane, J. Whiting, K. Chou, On thermal properties of metallic powder in laser powder bed fusion additive manufacturing, J. Manuf. Process. 47 (2019) 382–392.
- [30] L. Yang, K. Hsu, B. Baughman, D. Godfrey, F. Medina, M. Menon, S. Wiener, Additive Manufacturing Technologies: Rapid Prototyping to Direct Digital Manufacturing, Springer International Publishing, NY, 2017.
- [31] S.S. Djokić (Ed.), Electrochemical Production of Metal Powders, Springer Science + Business Media New York, 2012.
- [32] I. Gibson, D.W. Rosen, B. Stucker, Additive Manufacturing Technologies: Rapid Prototyping to Direct Digital Manufacturing, Springer Science + Business Media, NY, 2015.
- [33] T.D. Ngo, A. Kashani, G. Imbalzano, K.T.Q. Nguyen, D. Hui, Additive manufacturing (3D printing): a review of materials, methods, applications and challenges, Compos. Part B Eng. 143 (2018) 172–196.
- [34] S. Singh, S. Ramakrishna, R. Singh, Material issues in additive manufacturing: a review, J. Manuf. Process. 25 (2017) 185–200.
- [35] N. Li, S. Huang, G. Zhang, R. Qin, W. Liu, H. Xiong, G. Shi, J. Blackburn, Progress in additive manufacturing on new materials: a review, J. Mater. Sci. Technol. (2018).
- [36] P. Parandoush, D. Lin, A review on additive manufacturing of polymer-fiber composites, Compos. Struct. 182 (2017) 36–53.
- [37] O.O. Ajibola, D.T. Oloruntoba, B.O. Adewuyi, Effects of moulding sand permeability and pouring temperatures on properties of cast 6061 aluminium alloy, Int. J. Met. 2015 (2015) 13.
- [38] S. Ahmad, S. Puri, S.K. Das, Phase separation of fluids in porous media: a molecular dynamics study, Phys. Rev. E 90 (4) (2014) 040302.
- 39] J.P. Herzig, D.M. Leclerc, P.L. Goff, Flow of suspensions through porous media—application to deep filtration, Ind. Eng. Chem. 62 (5) (1970) 8–35.
- [40] B.I. Pavel, A.A. Mohamad, An experimental and numerical study on heat transfer enhancement for gas heat exchangers fitted with porous media, Int. J. Heat Mass Transf. 47 (23) (2004) 4939–4952.
- [41] C. Sander, P. Holm, Porous magnesium aluminometasilicate tablets as carrier of a cyclosporine self-emulsifying formulation, AAPS PharmSciTech 10 (4) (2009) 1388.
- [42] G.R. Klinzing, A. Zavaliangos, A simplified model of moisture transport in hydrophilic porous media with applications to pharmaceutical tablets, J. Pharm. Science 105 (8) (2016) 2410–2418.
- [43] J.F. Allard, Acoustic impedance at Normal incidence of fluids, and highly porous materials, Propagation of Sound in Porous Media: Modelling Sound Absorbing Materials, Springer Netherlands, Dordrecht, 1993, pp. 16–30.
- [44] N. Gupta, E. Woldesenbet, P. Mensah, Compression properties of syntactic foams: effect of cenosphere radius ratio and specimen aspect ratio, Compos. Part A Appl.

- Sci. Manuf. 35 (1) (2004) 103-111.
- [45] O. Koutný, J. Kratochvíl, J. Švec, J. Bednárek, Modelling of packing density for particle composites design, Procedia Eng. 151 (2016) 198–205.
- [46] J. Zhang, M.F. Ashby, Mechanical selection of foams and honeycombs used for packaging and energy absorption, J. Mater. Sci. 29 (1) (1994) 157–163.
- [47] D.A. Nield, A. Bejan, Mass transfer in a porous medium: multicomponent and multiphase flows, Convection in Porous Media, Springer New York, New York, NY, 1992, pp. 29–46.
- [48] S. Torquato, T.M. Truskett, P.G. Debenedetti, Is random close packing of spheres well defined? Phys. Rev. Lett. 84 (10) (2000) 2064.
- [49] S. Vaucher, E. Carreño-Morelli, C. André, O. Beffort, Selective laser sintering of aluminium- and titanium-based composites: processing and characterisation, Phys. Status Solidi 199 (3) (2003) R11–R13.
- [50] D. Lin, C. Richard Liu, G.J. Cheng, Single-layer graphene oxide reinforced metal matrix composites by laser sintering: microstructure and mechanical property enhancement, Acta Mater. 80 (2014) 183–193.
- [51] D. Gu, Particle-reinforced Cu matrix composites by direct metal laser sintering (DMLS) additive manufacturing (AM): interface design, material optimization, and process control, Laser Additive Manufacturing of High-Performance Materials, Springer Berlin Heidelberg, Berlin, Heidelberg, 2015, pp. 223–272.
- [52] Q. Han, Y. Geng, R. Setchi, F. Lacan, D. Gu, S.L. Evans, Macro and nanoscale wear behaviour of Al-Al2O3 nanocomposites fabricated by selective laser melting, Compos. Part B Eng. 127 (Supplement C) (2017) 26–35.
- [53] B.W. Xiong, H. Yu, Z.F. Xu, Q.S. Yan, Y.H. Zheng, P.L. Zhu, S.N. Chen, Study on dual binders for fabricating SiC particulate preforms using selective laser sintering, Compos. Part B Eng. 48 (Supplement C) (2013) 129–133.
- [54] R. McGeary, Mechanical packing of spherical particles, J. Am. Ceram. Soc. 44 (10) (1961) 513–522.
- [55] J. Bernal, J. Mason, Packing of spheres: co-ordination of randomly packed spheres, Nature 188 (4754) (1960) 910–911.
- [56] C. Song, P. Wang, H.A. Makse, A phase diagram for jammed matter, Nature 453 (7195) (2008) 629–632.
- [57] ASTM, Standard Test Methods for Maximum Index Density and Unit Weight of Soils Using a Vibratory Table. 2016, ASTM International, West Conshohocken, PA, 2016.
- [58] ASTM, Standard Practice for Classification of Soils for Engineering Purposes (Unified Soil Classification System), ASTM International, West Conshohocken, PA, 2011.
- [59] G. Scott, D. Kilgour, The density of random close packing of spheres, J. Phys. D Appl. Phys. 2 (6) (1969) 863.
- [60] R. German, Particle Packing Characteristics, Metal Powder Industries Federation, Princeton, New Jersey, 1989.
- [61] R. Benenati, C. Brosilow, Void fraction distribution in beds of spheres, Aiche J. 8 (3) (1962) 359–361.
- [62] A. De Klerk, Voidage variation in packed beds at small column to particle diameter ratio, Aiche J. 49 (8) (2003) 2022–2029.
- [63] L.C. Graton, H. Fraser, Systematic packing of spheres: with particular relation to porosity and permeability. J. Geol. 43 (8. Part 1) (1935) 785–909.
- [64] A. Yu, N. Standish, An analytical—parametric theory of the random packing of particles, Powder Technol. 55 (3) (1988) 171–186.
- [65] A.R. Kansal, S. Torquato, F.H. Stillinger, Diversity of order and densities in jammed hard-particle packings, Phys. Rev. E 66 (4) (2002) 041109.
- [66] A.B. Hopkins, F.H. Stillinger, S. Torquato, Disordered strictly jammed binary sphere packings attain an anomalously large range of densities, Phys. Rev. E 88 (2) (2013) 022205
- [67] A.J. Poslinski, M.E. Ryan, R.K. Gupta, S.G. Seshadri, F.J. Frechette, Rheological behavior of filled polymeric systems II. The effect of a bimodal size distribution of particulates, J. Rheol. 32 (8) (1988) 751–771.
- [68] J. Spangenberg, G.W. Scherer, A.B. Hopkins, S. Torquato, Viscosity of bimodal suspensions with hard spherical particles, J. Appl. Phys. 116 (18) (2014) 184902.
- [69] C.-J. Bae, J.W. Halloran, Concentrated suspension-based additive manufacturing viscosity, packing density, and segregation, J. Eur. Ceram. Soc. 39 (14) (2019) 4299–4306.
- [70] R. Fedors, R. Landel, An empirical method of estimating the void fraction in mixtures of uniform particles of different size, Powder Technol. 23 (2) (1979) 225–231.
- [71] C. Furnas, Grading aggregates-I.-Mathematical relations for beds of broken solids of maximum density, Ind. Eng. Chem. 23 (9) (1931) 1052–1058.
- [72] A.R. Westman, H. Hugill, The packing of particles, J. Am. Ceram. Soc. 13 (10) (1930) 767–779.
- [73] A.E.R. Westman, The packing of particles: empirical equations for intermediate diameter ratios, J. Am. Ceram. Soc. 19 (1-12) (1936) 127–129.
- [74] A. Yu, N. Standish, Porosity calculations of multi-component mixtures of spherical particles, Powder Technol. 52 (3) (1987) 233–241.
- [75] K. Ridgway, K. Tarbuck, Voidage fluctuations in randomly-packed beds of spheres adjacent to a containing wall, Chem. Eng. Sci. 23 (9) (1968) 1147–1155.
- [76] K. Ridgway, K.J. Tarbuck, Radial voidage variation in randomly-packed beds of spheres of different sizes, J. Pharm. Pharmacol. 18 (S1) (1966) 168S–175S.
- [77] H. Scheffé, Experiments with mixtures, J. R. Stat. Soc. Ser. B (1958) 344-360.
- [78] R. Jeschar, W. Potke, V. Petersen, K. Polthier, Blast furnace aerodynamics, Proceedings of the Symposium on Blast Furnace Aerodynamics, Sept., 1975.
- [79] G. Eshel, G.J. Levy, U. Mingelgrin, M.J. Singer, Critical evaluation of the use of laser diffraction for particle-size distribution analysis, Soil Sci. Soc. Am. J. 68 (3) (2004) 736–743.
- [80] X.S. Wang, V. Palero, J. Soria, M.J. Rhodes, Laser-based planar imaging of nanoparticle fluidization: part II—mechanistic analysis of nanoparticle aggregation,

- Chem. Eng. Sci. 61 (24) (2006) 8040-8049.
- [81] H.Y. Sohn, C. Moreland, The effect of particle size distribution on packing density, Can. J. Chem. Eng. 46 (3) (1968) 162–167.
- [82] A. Santos, S.B. Yuste, M.L. de Haro, G. Odriozola, V. Ogarko, Simple effective rule to estimate the jamming packing fraction of polydisperse hard spheres, Phys. Rev. E 89 (4) (2014) 040302.
- [83] K.W. Desmond, E.R. Weeks, Influence of particle size distribution on random close packing of spheres, Phys. Rev. E 90 (2) (2014) 022204.
- [84] A. Yu, R. Zou, N. Standish, Modifying the linear packing model for predicting the porosity of nonspherical particle mixtures, Ind. Eng. Chem. Res. 35 (10) (1996) 3730–3741.
- [85] A. Yu, N. Standish, Characterisation of non-spherical particles from their packing behaviour, Powder Technol. 74 (3) (1993) 205–213.
- [86] A. Yu, J. Bridgwater, A. Burbidge, On the modelling of the packing of fine particles, Powder Technol. 92 (3) (1997) 185–194.
- [87] S. Williams, A. Philipse, Random packings of spheres and spherocylinders simulated by mechanical contraction, Phys. Rev. E 67 (5) (2003) 051301.
- [88] M. Marek, A study of geometrical structure of packed beds using flow simulation with the immersed boundary method, J. Phys. Conf. Ser. 760 (1) (2016) 012016.
- [89] P.Y. Lanfrey, Z.V. Kuzeljevic, M.P. Dudukovic, Tortuosity model for fixed beds randomly packed with identical particles, Chem. Eng. Sci. 65 (5) (2010) 1891–1896
- [90] A. Donev, I. Cisse, D. Sachs, E.A. Variano, F.H. Stillinger, R. Connelly, S. Torquato, P.M. Chaikin, Improving the density of jammed disordered packings using ellipsoids, Science 303 (5660) (2004) 990–993.
- [91] Z.-Y. Zhou, R.-P. Zou, D. Pinson, A.-B. Yu, Dynamic simulation of the packing of Ellipsoidal Particles, Ind. Eng. Chem. Res. 50 (16) (2011) 9787–9798.
- [92] J. Gan, Z. Zhou, A. Yu, Particle scale study of heat transfer in packed and fluidized beds of ellipsoidal particles, Chem. Eng. Sci. 144 (2016) 201–215.
- [93] A. Wouterse, S.R. Williams, A.P. Philipse, Effect of particle shape on the density and microstructure of random packings, J. Phys. Condens. Matter 19 (40) (2007) 406215.
- [94] M. Kou, H. Zhou, S. Wu, Y. Shen, DEM simulation of cubical particle percolation in a packed bed, Powder Technol. (2019).
- [95] F. Dolamore, C. Fee, S. Dimartino, Modelling ordered packed beds of spheres: the importance of bed orientation and the influence of tortuosity on dispersion, J. Chromatogr. A 1532 (2018) 150–160.
- [96] F. Meng, M. Elsahati, J. Liu, R.F. Richards, Thermal resistance between amorphous silica nanoparticles, J. Appl. Phys. 121 (19) (2017) 194302.
- [97] R.K. Cersonsky, G. van Anders, P.M. Dodd, S.C. Glotzer, Relevance of packing to colloidal self-assembly, Proc. Natl. Acad. Sci. 115 (7) (2018) 1439–1444.
- [98] S. Mutsers, K. Rietema, The effect of interparticle forces on the expansion of a homogeneous gas-fluidized bed, Powder Technol. 18 (2) (1977) 239–248.
- [99] K. Yen, T. Chaki, A dynamic simulation of particle rearrangement in powder packings with realistic interactions, J. Appl. Phys. 71 (7) (1992) 3164–3173.
- [100] T.M. Wischeropp, C. Emmelmann, M. Brandt, A. Pateras, Measurement of actual powder layer height and packing density in a single layer in selective laser melting, Addit. Manuf. 28 (2019) 176–183.
- [101] H.W. Mindt, M. Megahed, N.P. Lavery, M.A. Holmes, S.G.R. Brown, Powder bed layer characteristics: the overseen first-order process input, Metall. Mater. Trans. A 47 (8) (2016) 3811–3822.
- [102] N.E. Gorji, R. O'Connor, A. Mussatto, M. Snelgrove, P.G.M. González, D. Brabazon, Recyclability of stainless steel (316 L) powder within the additive manufacturing process, Materialia 8 (2019) 100489.
- [103] N.E. Gorji, R. O'Connor, D. Brabazon, XPS, XRD, and SEM characterization of the virgin and recycled metallic powders for 3D printing applications, IOP Conf. Series: Materials Science and Engineering 591 (2019) 012016.
- [104] P. Carroll, A. Pinkerton, J. Allen, W. Syed, H. Sezer, P. Brown, G. Ng, R. Scudamore, L. Li, The effect of powder recycling in direct metal laser deposition on powder and manufactured part characteristics, (2006).
- [105] V. Seyda, N. Kaufmann, C. Emmelmann, Investigation of aging processes of Ti-6Al-4 V powder material in laser melting, Phys. Procedia 39 (2012) 425–431.
- [106] J. Dawes, R. Bowerman, R. Trepleton, Introduction to the additive manufacturing powder metallurgy supply chain, Johnson Matthey Technol. Rev. 59 (3) (2015) 243–256
- [107] H. Niu, I. Chang, Selective laser sintering of gas and water atomized high speed steel powders, Scr. Mater. 41 (1) (1999) 25–30.
- [108] D. Manfredi, F. Calignano, M. Krishnan, R. Canali, E.P. Ambrosio, E. Atzeni, From powders to dense metal parts: characterization of a commercial AlSiMg alloy processed through direct metal laser sintering, Materials 6 (3) (2013) 856–869.
- [109] T. Ogihara, T. Kubo, S. Arita, N. Aoyagi, R. Ueyama, M. Harada, A. Harada, Production and characterization of silver powder created using high-pressure water atomization, J. Ceram. Soc. Jpn. 125 (1) (2017) 19–22.
- [110] A. Simchi, The role of particle size on the laser sintering of iron powder, Metall. Mater. Trans. B 35 (5) (2004) 937–948.
- [111] A. Spierings, G. Levy, Comparison of density of stainless steel 316L parts produced with selective laser melting using different powder grades, Proceedings of the Annual International Solid Freeform Fabrication Symposium, (2009) Austin, TX.
- [112] N.D. Parab, J.E. Barnes, C. Zhao, R.W. Cunningham, K. Fezzaa, A.D. Rollett, T. Sun, Real time observation of binder jetting printing process using high-speed X-ray imaging, Sci. Rep. 9 (1) (2019) 2499.
- [113] A. Lores, N. Azurmendi, I. Agote, E. Zuza, A review on recent developments in binder jetting metal additive manufacturing: materials and process characteristics, Powder Metall. 62 (5) (2019) 267–296.
- [114] H. Miyanaji, Effect of powder characteristics on parts fabricated via binder jetting process, Rapid Prototyp. J. 25 (2) (2019) 332–342.

- [115] A. Simchi, Direct laser sintering of metal powders: mechanism, kinetics and microstructural features, Mater. Sci. Eng. A 428 (1) (2006) 148–158.
- [116] B. Liu, R. Wildman, C. Tuck, I. Ashcroft, R. Hague, Investigation the effect of particle size distribution on processing parameters optimisation in selective laser melting process, Additive Manufacturing Research Group, Loughborough University (2011).
- [117] A.B. Spierings, N. Herres, G. Levy, Influence of the particle size distribution on surface quality and mechanical properties in AM steel parts, Rapid Prototyp. J. (2011) 195–202.
- [118] D. Zhang, W. Wang, Y. Guo, S. Hu, D. Dong, R. Poprawe, J.H. Schleifenbaum, S. Ziegler, Numerical simulation in the absorption behavior of Ti6Al4V powder materials to laser energy during SLM, J. Mater. Process. Technol. 268 (2019)
- 25-36
- [119] C.D. Boley, S.A. Khairallah, A.M. Rubenchik, Calculation of laser absorption by metal powders in additive manufacturing, Appl. Opt. 54 (9) (2015) 2477–2482.
- [120] C.D. Boley, S.C. Mitchell, A.M. Rubenchik, S.S.Q. Wu, Metal powder absorptivity: modeling and experiment, Appl. Opt. 55 (23) (2016) 6496–6500.
- [121] L. Dai, V. Sorkin, G. Vastola, Y.W. Zhang, Dynamics calibration of particle sandpile packing characteristics via discrete element method, Powder Technol. 347 (2019) 220–226.
- [122] H. Chen, Q. Wei, Y. Zhang, F. Chen, Y. Shi, W. Yan, Powder-spreading mechanisms in powder-bed-based additive manufacturing: experiments and computational modeling, Acta Mater. 179 (2019) 158–171.